1 Exometabolite dynamics over stationary phase reveal strain-specific responses

3 John L. Chodkowski¹ and Ashley Shade^{1,2,3*}

- ¹Department of Microbiology and Molecular Genetics, Michigan State University, East
- 6 Lansing, MI 48824, USA
- ²Department of Plant, Soil and Microbial Sciences, Michigan State University, East
- 8 Lansing, MI 48824, USA
- ⁹ Program in Ecology, Evolutionary Biology and Behavior, Michigan State University,
- 10 East Lansing, MI 48824, USA

*Corresponding author and material requests. Email: shadeash@msu.edu

Abstract

Microbial exponential growth is expected to occur infrequently in environments that have long periods of nutrient starvation punctuated by short periods of high nutrient flux. These conditions likely impose non-growth states for microbes. However, non-growth states are uncharacterized for the majority of environmental bacteria, especially in regard to exometabolite production. We compared exometabolites produced over stationary phase across three environmental bacteria: *Burkholderia thailandensis* E264 (ATCC 700388), *Chromobacterium violaceum* ATCC 31532, and *Pseudomonas syringae* pathovar *tomato* DC3000 (ATCC BAA-871). We grew each strain in monoculture and investigated exometabolite dynamics from mid-exponential to stationary phase. We focused on exometabolites that were released into the media and accumulated over 45 hours, including approximately 20 hours of stationary phase. We

also analyzed transcripts (RNA-seq) to interpret exometabolite output. We found that a majority of exometabolites released were strain-specific, with a subset of identified exometabolites involved in both central and secondary metabolism. Transcript analysis supported that exometabolites were released from intact cells, as various transporters had either increased or consistent transcripts through time. Interestingly, we found that succinate was one of the most abundant identifiable exometabolites for all strains, and that each strain re-routed their metabolic pathways involved in succinate production during stationary phase. These results show that non-growth states can be metabolically dynamic, and that environmental bacteria can enrich a minimal environment with diverse chemical compounds as a consequence of growth and post-growth maintenance in stationary phase. This work provides insights into microbial community interactions via exometabolites in conditions of growth cessation or limitation.

Importance

Non-growth states are common for bacteria that live in environments that are densely populated and predominantly nutrient exhausted, and yet these states remain largely uncharacterized in cellular metabolism and metabolite output. Here, we investigated and compared stationary phase exometabolites and RNA transcripts for each of three environmental bacterial strains. We observed that diverse exometabolites were produced and provide evidence that these exometabolites accumulate over time through the release by intact cells. Additionally, each bacteria strain had a characteristic exometabolite profile and exhibited dynamics in exometabolite composition. This work

affirms that stationary phase is metabolically dynamic, with each strain tested creating a unique chemical signature in the extracellular space and altering metabolism in stationary phase. These findings set the stage for understanding how bacterial populations can support surrounding neighbors in environments with prolonged nutrient exhaustion through exometabolite-mediated interspecies interactions.

Keywords

Burkholderia thailandensis, Chromobacterium violaceum, Pseudomonas syringae, secondary metabolism, RNA-seq, mass spectrometry, metabolomics, stationary phase, non-growth state

Introduction

Much of microbiology research in the laboratory is conducted with bacterial or archaeal populations that are growing exponentially. However, it is estimated that 60% of microbial biomass in the environment is in a non-growing state (1, 2). Non-growing states can arise by virtue of being dormant (e.g. low metabolic activity) or entering stationary phase (e.g. maintenance-levels of metabolic activity) (3), where the latter refers to a population-level phenomenon that occurs after exponential growth. Various abiotic and biotic stressors at carrying capacity are known to induce stationary phase including nutrient exhaustion/inaccessibility and the accumulation of waste products. Particular environments impose conditions where microbial populations are in stationary phase for a better part of their existence. For example, dry soils with intermittent periods of rewetting (4–6), activated sludge operating in a sequencing batch reactor (SBR) (7,

8), and in the human gut (9, 10). Thus, unlike most cultivated laboratory strains, microbes experience stationary phase in environments where short periods of high nutrient flux is followed by long periods of famine (11, 12).

Bacteria survive in stationary phase by employing various stress response adaptations (13–15). Stress response adaptations include changes to cell morphology, transcription, translation, and metabolism. Furthermore, in stationary phase, microbes can re-route metabolic pathways to maintain essential components of the cell and the proton motive force (16). While these adaptations are thought to serve as survival mechanisms, the levels and types of metabolic activities in stationary phase are not well understood for most environmental microbes.

It is known, however, that microbes can exhibit appreciable metabolic activity in stationary phase (17). For example, entry into stationary phase resulted in prolonged protein production in *Escherichia coli* despite a decrease in overall protein levels (18). Metabolomic studies of *E. coli* in stationary phase support that there are unique metabolite production profiles associated with metabolic responses to growth arrest (19–21). These studies have provided valuable insights into stationary phase physiology. However, metabolome studies of microorganisms have generally focused on the dynamics of intracellular metabolites. It is expected that understanding metabolite dynamics in the extracellular environment can provide insights into metabolic responses that are relevant for microbial communities and interactions amongst coexisting community members.

Exometabolomics is the characterization of small, extracellular molecules either released by a microbe through means of lysis or diffusion, passive or active (22).

Characterizing exometabolites can provide insights into the potential for microbes to engage locally with other microbes and the environment via release of small molecules (23). The effect of these small molecules on neighboring microbes can range from cooperative (e.g. signaling molecules) to antagonistic (e.g. antibiotics) (24). Some exometabolites, such as antibiotics, are known to increase in production upon entry into stationary phase (15). In addition, computational models have predicted that costless exometabolite production, such intermediates of central carbon metabolism, may be common among bacteria (25), which could provide an overall benefit in a microbial community setting. Untargeted exometabolomic profiling has benefited from recent advances in the sensitivity and throughput of mass spectrometers (26). This approach provides an experimental basis to observe the breadth of exometabolites produced by microbial strains and strain-specific contributions to the exometabolite pool. Characterizing the exometabolite profile of a microbial population over time can be applied to understand the dynamic interplay between cell metabolism and the environment. Integrating untargeted exometabolomic approaches with other 'omic technologies (e.g. transcriptomics, genomics) informs comparisons across microbial populations of their metabolic responses in stationary phase.

95

96

97

98

99

100

101

102

103

104

105

106

107

108

109

110

111

112

113

114

115

116

117

We present an investigation of three environmental bacterial strains that are commonly associated with terrestrial environments (soils or plants) (Table 1). These strains were chosen because of reported (27) and observed interspecies exometabolite interactions in the lab. This current study evaluated exometabolite production for each strain in monoculture to first establish typical single-strain responses over stationary phase, with goals to next proceed to understand exometabolite-mediated interactions

among strains. Our previous work established a robust and flexible approach to investigate microbial exometabolite production in either monoculture or co-culture (28). Our approach uses filter plates that allow for the separation of cells from an exometabolite reservoir. Here, we examined the detailed exometabolite and transcript dynamics, defined as compositional changes through time, for each of these three environmental strains in monoculture over stationary phase after growth in minimal glucose (3.7 mM) medium. We asked: What is the diversity of unique exometabolites that accumulate over stationary phase? What is a likely explanation (e.g. transport from viable cells or lysis) for the accumulation of exometabolites? How does exometabolite composition and production compare across strains and time, and what general insights could these provide for understanding microbial metabolism and ecology of stationary phase?

We found that exometabolite composition is dynamic through stationary phase, and that accumulated exometabolites were likely released from intact cells. We also found that a majority of released exometabolites were strain-specific, suggesting that different bacterial strains have individualized responses to stationary phase. Finally, we found that all three strains re-routed metabolism in stationary phase.

Results

Each strain had a distinct exometabolite profile in stationary phase

In total, 10,352 features were detected by mass spectral analysis (Fig. 1, Table 2) across the three strains. These features represent what we defined as released exometabolites (see Methods: Mass spectrometry analysis section). Briefly, released exometabolites were defined as those that had temporal accumulation (assessed via

peak area) in stationary phase. Most features detected were strain-specific, and the number of unique features from any one strain outnumbered the total number of features shared by at least two strains (1494 features, ~16.9%). Of the 1494 shared features, ~12.7% were shared among all three strains. Specifically, *B. thailandensis* had the most unique detected features (~41.8%), followed by *P. syringae* (~25.2%) and *C. violaceum* (~18.6%) compared to all detected features. These data suggest that, despite monoculture growth in minimal medium initially containing one carbon source, an abundance of strain-specific exometabolites are produced during stationary phase.

We were interested in understanding differences in exometabolite composition and exometabolite temporal dynamics over stationary phase (Fig. 2). Comparing across strains (Fig. 2A-D), each strain had strain-specific exometabolite profiles (Adonis 0.590 $\leq r^2 \leq 0.808$, P value ≤ 0.001 , all pair-wise FDR-adjusted P values ≤ 0.001). For each strain, exometabolite profiles from exponential growth phase were distinct from stationary phase profiles (Fig 2). Strain differences in released exometabolites were more important than time in explaining variation in exometabolite composition on both PCoA axes. As expected, strain identity explained $\geq 57\%$ of the variation while time explained $\leq 6\%$ of the variation across all polarity/ionization modes (Supplementary Table S1). However, the most variation was explained by the interaction effect of strain x time (Supplementary Table S1).). Thus, exometabolite compositional differences were mainly driven by the different released exometabolites by the different strains. This was expected given the large number of unique features detected for each strain (Table 2).

Alternatively, we further looked at the influence of time on exometabolite profiles by observing exometabolites released by each strain, separately. We considered only

those exometabolites that met our stringent criteria for release and accumulation over time (see Methods). Notably, with these criteria, some of the same exometabolites were classified as released for some strains but not for others. In these cases, exometabolites were excluded from the temporal analysis of any strains for which the release criteria were not met. Directional temporal dynamics was observed for each strain (Fig. 2E-G), though continued directionality was not observed in some of the latest time points (e.g. Fig. 2F). We define directional as a progressive, step-wise trajectory between time points, where each time point is distinguished from any of the previous time points, and even more distinct from previous time points in PCoA space. This ultimately reflects temporal changes in exometabolite composition. Temporal trajectories in exometabolite profiles were highly reproducible for each strain across biological replicates (Protest analyses, Supplementary Table S2). For all strains, the difference between exometabolite profiles progressively increased when comparing each stationary phase time point to the initial, exponential phase time point (Supplementary Table S3). But, comparing successive time points revealed that the greatest differences occurred between the first stationary phase time point and the exponential phase time point. Notably, dissimilarity decreased between successive time points in stationary phase such that the latest time points were more similar to each other than the earliest time points (Supplementary Table S4). For each strain, the exometabolite profile changed over time (Supplementary Table S5). However, this was primarily due to differences in exometabolite profiles when comparing the exponential phase time point to each of the stationary phase time points (Supplementary Table S6). We note that hundreds to thousands of features were detected in late stationary phase

164

165

166

167

168

169

170

171

172

173

174

175

176

177

178

179

180

181

182

183

184

185

186

but were excluded (see Methods: Mass spectrometry analysis section) from the final dataset of released exometabolites. We maintained strict criteria for the detection of and accumulation of released exometabolites over stationary phase. Taken together, these data suggest that differences in exometabolite composition are largely driven by strain-specific production of exometabolites. Accounting for all released exometabolites within each strain, similar temporal patterns emerge, with the largest differences observed between exponential phase and stationary phase and more subtle differences observed over consecutive time points within stationary phase.

187

188

189

190

191

192

193

194

195

196

197

198

199

200

201

202

203

204

205

206

207

208

209

Hierarchal clustering analysis also revealed strain-specific features and their dynamics (Fig. 3). Most features across all strains reached maximum accumulation in late stationary phase. Notably, exometabolites accumulated despite generally steady strain population levels (Supplementary Fig. S1). We did observe ~1 generation in B. thailandensis and P. syringae over the course of stationary phase but the doubling took 20 h to complete. Dead cells across the time series remained consistent for both *B*. thailandensis and C. violaceum but increased for P. syringae (Supplementary Fig. S1). However, the quantity of live cells remained higher than the quantity of dead cells across the time series for all strains. Largely consistent counts of viable cells and a lack of death phase suggest that many exometabolites were released by intact cells rather than by lysis. To add support to this hypothesis, transcriptomics data indicate multiple organic molecule transporters were either consistently expressed throughout the time series or differentially expressed (Table 3, Dataset 1). Notable examples for all strains include various transporters related to dipeptide and C-4 dicarboxylate transport. In summary, despite growth arrest, each bacterial strain continued to produce (and the

media accumulated) a distinctive and dynamic profile of exometabolites into stationary phase.

Identity of stationary phase exometabolites

Of the total set of exometabolite features, only 188 (~1.8%) could be identified (Fig. 4, Supplementary Figs. S2-S4, <u>Dataset 2</u>). These were classified according to the Metabolomics Standards Initiative (MSI): MSI level 1 (Identified compounds) and MSI level 2 (putatively identified compounds). Most of the identified exometabolites were uniquely produced by one strain under our experimental conditions, though there were some exometabolites shared across strains, especially between *C. violaceum* and *P. syringae* (<u>Dataset 2</u>). Many of the identified exometabolites, particularly those molecules involved in central metabolism, such as amino acids, nucleotides/nucleosides, and carboxylic acids, were classified using an in-house standard in accordance with MSI level 1. In addition, MSI level 1 exometabolites such as ectoine, proline, trehalose, and glutamate likely indicated a cellular stress (e.g. osmotic stress).

Exometabolites putatively identified at MSI level 2 were annotated by matching MS/MS fragmentation to a reference database. MSI level 2 exometabolites included secondary metabolites such as bactobolin, yersiniabactin, and acyl homoserine lactones (AHLs) produced by *B. thailandensis*, *P. syringae*, and *C. violaceum*, respectively. Bactobolin and yersiniabactin are bioactive molecules, previously characterized as a bacteriostatic antibiotic (29) and a siderophore/virulence factor (30), respectively. AHLs induce quorum sensing in *C. violaceum*, and are linked to the production of hydrogen cyanide, antibiotics, and proteases (31, 32). These putatively identified secondary exometabolites suggest that stationary phase is coordinated with

shifts in metabolism, priming strains for competition via chemical warfare or nutrient scavenging. These data also suggest that a competitive phenotype may be standard among bacteria even in the absence of non-kin competitors, suggesting either priming for interspecific competition or engagement in intraspecific competition. This competitive priming is also supported by the observation of increased transcripts for transport systems involved in competition. For example, competitive transport systems included the type III secretion system in *B. thailandensis* and multidrug efflux systems for both *C.* violaceum and P. syringae. When comparing transcripts between times 45h to 12.5h, the aforementioned transport systems had a log₂-fold change (LFC) in expression > 1. (<u>Dataset 1</u>). Finally, a large proportion of MSI level 2 exometabolites were dipeptides, suggesting either the degradation of proteins (14) or the formation of dipeptides by nonribosomal peptide synthetases (NRPS), found in biosynthetic gene clusters (<u>Dataset 3</u>). In summary, there was a consistent accumulation of a diversity of exometabolites in stationary phase, including exometabolites that were intermediates in central carbon metabolism as well as secondary metabolites implicated in competition.

233

234

235

236

237

238

239

240

241

242

243

244

245

246

247

248

249

250

251

252

253

254

255

To maximize annotation of remaining unidentified MS/MS data, we performed chemical ontology analysis to determine chemical classes of exometabolites produced in stationary phase. Using *in silico* prediction of exometabolites by MS/MS fragmentation patterns, we putatively characterized compound classes (MSI level 3 designation). Broadly, carboxylic acids and derivatives were the most abundant type of exometabolite produced in stationary phase for all strains (Fig. 5A). This is expected because carboxylic acid derivatives are prominent in cellular constituents and molecules involved in primary metabolism (e.g. TCA cycle). Their excess production, and release

to relieve internal accumulation, may be due to stoichiometric constraints in metabolic network topology (33). However, MSI level 3 exometabolites revealed considerable quantification of exometabolites related to fatty acyls, organonitrogen compounds, organooxygen compounds, and benzene and substituted derivatives, suggesting additional classes of exometabolites contributing to the exometabolite pool that are unable to be identified by MSI level 1 and level 2 standards. These chemical ontologies were resolved further to the direct parent level (Fig. 5B). Amino acids and peptides were the most abundant and common exometabolites across all identification levels. In particular, dipeptides were the most abundant exometabolite. Transcriptomics data also indicated that dipeptide transporters for each strain were either consistently expressed or differentially expressed over time (Table 3, Dataset 1). In summary, chemical ontology analysis revealed chemical classes represented in the exometabolite dataset but lacking identification and, revealed that dipeptides were a common exometabolite released by all strains.

Insights into stationary phase metabolic re-routing

We then aimed to interpret strain metabolism in stationary phase by focusing on exometabolites most confidently identified (MSI level 1). For each strain, we examined the 10 most abundant exometabolites that accumulated and were detected at the last time point (45 h) for positive and negative polar exometabolites. We included all MSI level 1 exometabolites in this analysis. Generally, the abundant, accumulated exometabolites that were distinct for each strain were also uniquely detected in those strains (Fig. 6, ANOVA, all Q-values ≤ 0.01), with two exceptions: 5'-methylthioadenosine and hypoxanthine were also abundant in *Chromobacterium*

violaceum media but not within its top 10 accumulated exometabolites. Transporters that had a log₂-fold change (LFC) in expression (comparing times 45h to 12.5h) > 1 could be linked with their substrates for both *C. violaceum* and *P. syringae* (Dataset 1). This included substrates such as succinate and cytosine for *C. violaceum* and *P. syringae*, respectively. None of the most abundant exometabolites in *B. thailandensis* could be linked to a transporter with a large LFC. The majority of strain-specific abundant exometabolites suggest that each strain released a set of unique metabolic intermediates into the extracellular environment. This finding could have implications for how bacterial populations maintain viability through interspecies interactions in periods of nutrient exhaustion. Perhaps a simple explanation for differences in the types of exometabolites released could result from differences in the alteration of stationary phase metabolism.

Of the most accumulated exometabolites, succinate was a common exometabolite detected in all strains, and this is unsurprising as it is directly involved in central metabolism. Notably, succinate did not meet our stringent definition of released and accumulating over stationary phase (Fig. 6). However, its abundance and accumulation for all strains and its important role in central metabolism warranted further investigation. We overlaid temporal log fold changes in gene expression onto KEGG pathways involved in succinate production (Fig. 7). These data suggest that all strains re-routed metabolism during stationary phase. For the most part, transcripts involved in glycolysis and the TCA were decreased in all strains (KEGG Pathways). With regard to succinate production, both *B. thailandensis* and *C. violaceum* appear to have re-routed metabolism to use the glyoxylate cycle, as supported by the increase in

transcripts for isocitrate lyase and increase in transcripts involved in the ß-oxidation of fatty acids. *P. syringae* appears to have re-routed metabolism to use the methylcitrate cycle to generate succinate, as evidenced by the increase in transcripts for 2-methylisocitrate lyase. Other potential sources of succinate production include the GABA shunt and succinyl-CoA:acetate CoA-transferase in both *B. thailandensis* and *P. syringae*. In all strains, stationary phase results in exometabolite production that appears to coincide with alterations in metabolism.

Discussion

Microbes can experience a feast-or-famine lifestyle in environments (e.g. soil, activated sludge, in the gut) where long periods of starvation are punctuated by short periods of nutrient flux (4–10). Thus, microbes in particular environments predominantly exist in stationary phase. Understanding the metabolic response to stationary phase can reveal generalities as well as strain-specific strategies to maintain viability in nutrient-exhausted environments.

We studied exometabolite production in stationary phase across three bacterial strains. We specifically focused our analyses on released exometabolites, metabolites that accumulated in the medium over time. Even though we applied a very conservative definition to identify features that accumulated over time, we detected and characterized thousands of features that met our criteria. However, in the end, only a subset of these features could be identified using standards, MS/MS databases, and computational

predictions based on chemical characteristics (Fig. 4, Supplementary Figs. S2-S4, <u>Dataset 2</u>).

323

324

325

326

327

328

329

330

331

332

333

334

335

336

337

338

339

340

341

342

343

344

345

Exometabolites could accumulate over stationary phase by two mechanisms. First, exometabolites could be transported passively or actively across viable cells' membranes. Second, cells could lyse and spill primary metabolites and other debris into extracellular environment (34). Our results suggest that a major contributing factor to exometabolite accumulation for all three strains investigated here was exometabolite release from intact cells. In fact, we did not observe a death phase over stationary phase (Supplementary Fig. S1). Live cells generally remained at consistent levels throughout stationary phase. One generation during stationary phase was observed for both *B. thailandensis* and *P. syringae*. Given the decrease in transcripts observed for multiple genes in central metabolism (KEGG Pathways), this generation was likely the result of reductive cell division (35–37). Dead cells were present and in particular, increased for *P. syringae* throughout the time course. While dead cells could leak exometabolites, the accumulation of certain exometabolites (e.g. secondary metabolites) were identified and have been previously associated with production from viable cells in stationary phase cultures from each strain (29, 30, 32) Furthermore, our results are consistent with a previous study in *E. coli* that observed the extracellular accumulation of nucleobases upon entry into stationary phase (19). Ribosome degradation is initiated in growth-limiting environments and is a likely source of nucleobase accumulation due to the degradation of rRNA (38). We also observed the accumulation of various nucleobases in the extracellular environment across all strains. consistent with the concept of some common stationary phase phenomenon among

bacteria. Additional evidence of exometabolite release from intact cells was provided by RNA-seg analysis. Transcriptomics results indicated the increase in transcripts for or consistent expression of transporters (Dataset 1). In a previous study, Paczia et al. also observed similar patterns of exometabolite accumulation in stationary phase in various strains (39). They were able to rule out lysis and determine that passive or active diffusion could explain exometabolite production in growth limited conditions. In integrating transcriptomics with exometabolomics, our study builds on the findings of Paczia et al. to identify transporters likely involved in exometabolite accumulation and to provide insights into alterations in stationary phase metabolism. Findings from our work and from Paczia et al. in agreement with metabolic models that suggest that the extracellular accumulation of central metabolites could be attributed to costless metabolic secretions in resource poor environments (25). Unintuitively, the release of exometabolites by viable cells, and, particularly, release of central carbon intermediates, may be a common adaptation of bacteria in stationary phase. An interesting explanation is that the stoichiometry of metabolites is constrained by evolved metabolic network topology: some metabolites could be produced in excess to meet all metabolite requirements for a bacterium. Fitness tradeoffs of metabolite overproduction (e.g. toxic accumulation) could be alleviated through metabolite efflux (33).

346

347

348

349

350

351

352

353

354

355

356

357

358

359

360

361

362

363

364

365

366

367

368

In addition to the characterization of exometabolites implicated in cooperative interactions (e.g. central carbon intermediates or quorum sensing molecules), we also identified exometabolites implicated in competition. An antibiotic (bactobolin), with previously described bioactivity (27, 29, 40), was produced by *B. thailandensis* and a siderophore/virulence factor (yersiniabactin) was produced by *P. syringae* (30),

representing interference (direct harm to neighbors) and exploitative (indirect negative interaction) competition strategies, respectively (41, 42). These exometabolites are involved in interspecies competition but, here, were produced in monoculture. While we did not identify an exometabolite in *C. violaceum* involved in competition, we did identify quorum sensing molecules, which are linked to the production of competitive exometabolites in this strain (31, 32). Taken together, the metabolic profile in each strain was altered in stationary phase and resulted in production of both cooperative and competitive exometabolites. Simultaneous production of both cooperative and competitive exometabolites may be an advantageous strategy to sustain kin while maintaining competition for scarce resources (25, 43). Additional studies that include co-coculturing experiments are needed to understand the impact that these exometabolites may have on ecological dynamics and these interplay of biotic factors under changing environmental conditions.

Putative (MSI level 2) exometabolite identifications provided evidence for the release of dipeptides (Fig. 5B) and transcriptomics provided evidence for differentially regulated or consistent expression of dipeptide transporters (<u>Dataset 1</u>). Hydrolysis by dipeptidyl peptidases of ribosomal proteins or degradation of other polypeptide chains can be one source of dipeptide production. Estimates in *E. coli* have shown that 50-80% of ribosomes were degraded upon transition from exponential phase to stationary phase (38). Interestingly, another source of dipeptides may be active production. Recent studies have examined dipeptide formation by adenylation domains in nonribosomal peptide synthetases (NRPS) (44, 45). All strains in our study have numerous NRPS that could contribute to the production of dipeptides (<u>Dataset 3</u>). Furthermore, one dipeptide

was characterized as a cyclic dipeptide. Cyclic dipeptides can be involved in cell communication (46). Thus, the diverse chemical ecology that can be facilitated by dipeptides points to the importance of understanding how dipeptides are formed and of characterizing the environments that induce their production.

A clear limitation to our study is in the incomplete exometabolite annotations.

Only 1.8% of released exometabolites could be identified. While exact molecule identifications are lagging behind the identification of new features, efforts have been put forth to chemically classify all MS/MS data (47). We used the same approach to computationally predict and classify the chemical ontology of MS/MS data not identified at MSI level 1 or level 2 (Fig. 5). Differences between *in silico* predictions of MS/MS data (MSI level 3) and MSI levels 1 and 2 was most apparent at the class level (Fig. 5A). This knowledge can be used to direct research efforts and analytical techniques to identify underrepresented classes of compounds. Targeted identification efforts of exometabolites will reveal uncharacterized biological phenomena occurring in experimental systems.

Microbes in growth-arrested states can re-route metabolism to maintain the proton motive force (PMF) and stabilize ATP levels (16). We used a combination of exometabolomics and transcriptomics to shed light on metabolic re-routing in each strain investigated. Notably, all three strains accumulated high levels of succinate, and this was further supported by RNA-seq data that showed an increase in transcripts in genes involved in succinate production (Fig. 7). We found that the major metabolic rerouting in stationary phase included transitioning to the glyoxylate cycle in *B. thailandensis* and *C. violaceum* and to the methylcitrate cycle in *P. syringae*. This

finding, specifically for B. thailandensis, agrees with previous studies in B. thailandensis and closely related strains. Previous studies found quorum-sensing mediated metabolic re-routing to the glyoxylate cycle during stationary phase in B. thailandensis and Burkholderia glumae as a mechanism to combat alkalinity toxicity (48, 49). Furthermore, the greatest increase in isocitrate lyase was observed in Burkholderia cenocepacia during stationary phase compared to other abiotic stressors (50). This supports the notion that a re-routing metabolism to the glyoxylate cycle in stationary phase may be a shared feature among members of the genus *Burkholderia*. Prior evidence for stationary phase metabolic re-routing in both *C. violaceum* and *P. syringae* is lacking. However, a metabolic model in C. violaceum ATCC 12472 suggested metabolic re-routing to the glyoxylate cycle occurred in response to antibiotics in a streptomycin-resistant population (51). In support of succinate extracellular accumulation, we found that C4dicarboxylic acid transporters were transcriptionally active in all three strains (Dataset 1). It could be that succinate export is facilitated by a succinate/proton symporter for maintenance of the PMF. However, both cycles involved in succinate production do not generate ATP, and the generation of ATP is are also necessary to maintain cell viability. While ATP could be generated through the production of acetate (Fig. 7), we note that we did not quantify acetate and therefore are unable to confirm this scenario. Additional studies are needed to confirm the mechanisms of maintaining cell viability during stationary phase. Regardless, combining exometabolomic and transcriptomic approaches provided increased biological interpretation that could not have been achieved by either approach in isolation. The characterization of exometabolite production and metabolic response to stationary phase in monocultures sets the stage

415

416

417

418

419

420

421

422

423

424

425

426

427

428

429

430

431

432

433

434

435

436

437

for understanding exometabolite-mediated interspecies interactions within a microbial community.

Materials and Methods

Bacterial strains and culture conditions

Glycerol stocks of *B. thailandensis*, *C. violaceum*, and *P. syringae* (Table 1) were plated on half-concentration Trypticase soy agar (TSA50) at 27°C for at least 24 h.

Strains were inoculated in 7 ml of M9–0.2% glucose medium and grown for 16 h at 27°C, 200 rpm. Cultures were then back-diluted into 50 ml M9-0.2% glucose medium such that exponential growth phase was achieved after 10 h of incubation at 27°C, 200 rpm. Strains were back-diluted in 50 ml M9–0.067% glucose medium to target ODs (*B. thailandensis* 0.3 OD, *C. violaceum*: 0.035 OD, *P. syringae* 0.035 OD) such that stationary phase was achieved after approximately 24 h of incubation in filter plates.

Filter plate experiments

We used the filter plate system to study each strain in monoculture over the course of stationary phase. Filter plate preparation was performed as previously described (28). Briefly, we used sterile filter plates with 0.22-µm-pore polyvinylidene difluoride (PVDF) filter bottoms (MultiScreen GV Filter Plate, 0.22 µm, MSGVS2210, Millipore). Prior to use, filter plates were washed three times with sterile water using a vacuum apparatus (NucleoVac 96 vacuum manifold; Clontech Laboratories). The filter of well H12 was removed with a sterile pipette tip and forceps, and 31 ml of M9–0.067% glucose medium was added to the reservoir through well H12. Each well was then filled with 130 µl of back-diluted culture in M9–0.067% glucose medium or medium only. For a given time series replicate, a custom R script (RandomArray.R [see the GitHub

repository]) was used to randomize the placement of a strain in the wells so that a strain occupied a total of 31 wells per plate and the remaining 64 wells were filled with medium. Each monoculture time course was independently replicated four times for a total of 12 experiments. The time course included 6 time points: an exponential phase point (12.5 h) and 5 points assessed every 5 h over stationary phase (25 h – 45 h). Plates were destructively sampled, comprising a total of 72 plates for the entire experimental design of 3 strains x 6 timepoints x 4 replicates.

Filter plates were incubated at 27°C with gentle shaking (~0.32 rcf). We again used our RandomArray.R script to randomize wells used for RNA extraction (16 wells, pooled per plate) and flow cytometry (5 wells, pooled per plate). During destructive sampling, first, the wells containing spent culture assigned to RNA-seq were pooled into a 1.5 mL microcentrifuge tube, flash frozen in liquid nitrogen, and stored at -80°C for RNA extraction. Next, wells containing spent culture assigned to flow cytometry were pooled, and then 20 μL was initially diluted in 180 μL Tris-buffered saline (TBS; 20 mM Tris, 0.8% NaCl [pH 7.4]), and then, after checking concentrations needed for accurate flow cytometry counts, diluted further in TBS to reach final dilutions of 1,300-fold, 1,540-fold, and 900-fold for *B. thailandensis*, *C. violaceum*, *P. syringae*, respectively. Finally, spent medium (~31 ml) from the shared reservoir was transferred into 50 mL conical tubes, flash-frozen in liquid nitrogen and stored at ~80 °C for subsequent exometabolite extraction.

Flow cytometry

Diluted cultures were stained with the Thermo Scientific LIVE/DEAD BacLight bacterial viability kit at final concentrations of 1.5 μ M Syto9 (live stain) and 2.5 μ M

propidium iodide (dead stain). Two hundred microliters of stained cultures were transferred to a 96-well microtiter U-bottom microplate (Thermo Scientific). Twenty microliters were analyzed on a BD Accuri C6 flow cytometer (BD Biosciences) at a fluidics rate of 66 µl/min and a threshold of 500 on an FL2 gate. The instrument contained the following optical filters: FL1-533, 30 nm; FL2-585, 40 nm; and FL3, 670-nm longpass. The counting accuracy of the flow cytometer was periodically checked with GFP beads. Data were analyzed using BD Accuri C6 software version 1.0.264.21 (BD Biosciences).

Metabolomics

LCMS sample preparation and data acquisition

The following methods were according to the Department of Energy Joint Genome Institute (DOE JGI) standard operating protocols performed at the DOE JGI facility. Spent medium samples from the monocultures were shipped from Michigan State to the DOE JGI overnight on dry ice. Spent medium (ranging from 2.5 to 8 mL) were lyophilized in a Labconoco FreeZone 2.5 lyophilizer (Labconco, Kansas City, MO). Dried samples were resuspended in 700 µL methanol, vortexed, sonicated for 10 minutes in a water bath (VWR Scientific Aquasonic Water Bath, Model 150HT), and then centrifuged for 2 minutes at 1200 g. Supernatant was transferred to 96 deep-well plate (1.1 mL) and then dried in a speed-vac (SPD111V, Thermo Scientific). Samples were stored at -80 °C until LC-MS analysis. Four extraction blanks were also prepared using the same protocol.

Dried samples were resuspended in methanol containing internal standards (ITSD). ITSD used for polar analysis were 13 C, 15 N amino acid mixture (30 μ M,

767964,Sigma, Inc). ITSD for nonpolar analysis was 2-Amino-3-bromo-5-methylbenzoic acid (ABMBA, 1 μg/mL). Additionally, a quality control (QC) sample containing ~20 common biomolecules was prepared. ITSD are used to check for injection errors, mass accuracy, and RT shifts within a sample. The m/z accuracy and retention time shifts in QC samples were assessed to check for instrument consistency and column performance. Samples were analyzed for both polar and non-polar exometabolites. Resuspended samples containing ITSD were vortexed, sonicated in a water bath for 2 minutes, transferred to transwell plates (MultiScreen GV Filter Plate, 0.22 μm, MSGVS2210, Millipore) and centrifuged for 2 min at ~1200 g into a 96-well plate, and then transferred into an LC-MS glass vial.

UHPLC chromatography was performed using and Agilent 1290 LC stack, with MS and tandem mass spectrometry (MS2) data collected in both positive and negative ion mode using a Thermo QExactive (for HILIC) or Thermo QExactive HF (for C18) mass spectrometer (Thermo Scientific, San Jose, CA). Full MS spectra was collected for m/z 80-1,200 at 60,000 resolution for C18, and m/z 70-1,050 at 70,000 resolution for HILIC. MS/MS fragmentation data was acquired using stepped collision energies between 10–40 eV at 17,500 resolution. Specifically, 1 MS1 scan was followed by 2 MS2 scans of the 2 most intense ions, then another MS1 scan followed by another 2 MS2 scans of the 2 most intense ions. If the 2 most intense ions were already fragmented in the previous 10 seconds of analysis, the next 2 most intense ions were fragmented. For MS2, 10,20 and 30eV collision energies were collected and averaged with the exception of one biological replicate per condition, where 10, 20 and 40eV collision energies were collected and averaged.

For detection of nonpolar metabolites, reverse phase chromatography was performed using a C18 column (Agilent ZORBAX Eclipse Plus C18, Rapid Resolution HD, 2.1 x 50 mm, 1.8 µm) at a flow rate of 0.4 mL/min. Samples were run on the C18 column held at 60 °C equilibrated with 100% buffer A (100% LC-MS water with 0.1 % formic acid) for 1 minute, followed by a linear gradient to 100% buffer B (100% acetonitrile with 0.1% formic acid) over 7 minutes, and then an isocratic elution in 100% buffer B for 1.5 minutes. A final re-equilibration to 100% buffer A over 1 minute and isocratic hold for 1 minute was performed prior to the next sample injection. For detection of polar metabolites, normal phase chromatography was performed using a ZICHydrophilic Interaction Liquid Chromatography (HILIC) column (SeQuant ZIC-HILIC) 3.5-µm particle size, 200 Å porosity, 150 mm x 2.1 mm, Millipore Sigma). Samples were run on the ZIC-HILIC column held at 40 °C equilibrated with 100% buffer B (95:5 acetonitrile:water with 5mM ammonium acetate) at a flow rate of 0.45 mL/min for 1.5 minutes, diluting buffer B down to 65% with buffer A (100% water with 5mM ammonium acetate) over 13.5 minutes, followed by a linear increase in flowrate to 0.6 mL/min as buffer B approached 0% over 3 minutes, and then an isocratic elution in 100% A for 5 minutes. This was followed by a 2 minute linear gradient back to 100% B and decrease in flowrate to 0.45 mL/min, and then a final 5 minute column re-equilibration at 100% B prior to the next sample injection.

530

531

532

533

534

535

536

537

538

539

540

541

542

543

544

545

546

547

548

549

550

551

552

Sample injection order on the mass spectrometer was randomized and an injection blank (2 uL of methanol) was run between each sample. For all samples, resuspension volume (70 to 120 μ L) and injection volume (2 μ L to 8 μ L) varied to normalize by initial sample volume prior to extraction. A total of 257 samples were

successfully analyzed (<u>Dataset 4</u>). Samples not included in downstream analyses were removed either because they failed quality standards during mass spectrometry analysis or the sample had low intragroup reproducibility.

Mass spectrometry analysis

Both MS and MS/MS data were used for untargeted metabolomics analysis. A total of 257/288 metabolomic samples were used for analysis ($\underline{Dataset\ 4}$); 30 samples were removed due to failed injection and 1 sample was removed due to low intragroup reproducibility in polar analysis (Pearson's $r \le 0.14$). MZmine (version 2.42) (52) was used for peak picking, aligning features across samples, and peak integration for both nonpolar and polar analyses and in both negative and positive ion mode. MZmine XML parameter files for all analyses can be viewed and downloaded from GitHub ($\underline{Dataset\ 7}$). For MS data, a feature by sample matrix was exported for additional feature filtering steps. For MS/MS data, the GNPS feature was used to export data in addition to performing a local spectra database search within MZmine (see Compound identification section, below).

We used filter featuring steps to identify exometabolites released from each strain in stationary phase. The feature filtering steps were performed as follows on a per-strain basis: 1) Features were removed if the max peak area was found in one of the replicates for the external control sample. 2) A noise filter: the minimum peak area of a feature from a replicate at the last time point (45 hr) needed to be 3X the maximum peak area of the same feature in one of the external control replicates. 3) Coefficient of variation (CV) values for each feature calculated between replicates at each time point needed to be less than 20% across the time series. 4) The minimum value of the

average peak area needed to be observed in the first, exponential phase time point (12.5 h). 5) The log₂ fold change of the average peak areas observed between the last (45 h) and first (12.5 h) timepoints needed to be greater than 1. 6) The time series abundance of a feature needed to have a Pearson correlation greater than or equal to 0.7.

Four final feature datasets from polar and nonpolar analysis in both ionization modes were analyzed in MetaboAnalyst 4.0 (53). Features were normalized by an internal standard (ITSD) reference feature (Dataset 5) and cube root transformed.

Reference features for polar analysis in positive (13C-15N-proline) and negative (13C-15N-alanine) was determined by the ITSD with the lowest CV value across all samples. The reference feature for nonpolar datasets was the ITSD 2-Amino-3-bromo-5-methylbenzoic acid (ABMBA). Heatmaps were generated in MetaboAnalyst using Ward's clustering algorithm with Euclidean distances from Z-scored data. Normalized and transformed datasets were exported from MetaboAnalyst to generate principal coordinate analysis (PCoA) plots in R. Abundances for exometabolites that did not pass release criteria in each strain were replaced with NAs prior to distance matrix computation.

Compound identification

A three step process was used to identify compounds or characterize chemical ontologies(47). Identification confidence was assigned according to the Metabolomics Standards Initiative (MSI) (54). First, compounds were identified by an in-house reference library at the Joint Genome Institute (JGI). This reference library was curated to identify compounds based on m/z, retention time, and MS/MS spectra of standards. A

compound passing the first two criteria were denoted MSI level 1. A compound passing all three criteria exceeded MSI level 1. All compounds at or exceeding MSI level 1 were identified using the reference library. This reference library was only available for polar analysis. Ranges for m/z and retention time values for compounds in the reference library were used to identify exometabolites from the MZmine analysis (Dataset 6).

We made an effort to identify as many of the remaining compounds from both polar and nonpolar analyses that had MS/MS data. MS/MS data acquired during mass spec analysis were used to putatively identify compounds that matched to fragmentation patterns from libraries outside of JGI; these were assigned MSI level 2. First, MS/MS data was exported to GNPS format and analyzed in GNPS (55) to match fragmentation patterns against the NIST17 commercial library. Second, a local spectra database search was performed within MZmine using the entire compound library from MassBank of North American (MoNA- https://mona.fiehnlab.ucdavis.edu). For both approaches, compounds were putatively identified if cosine scores were 0.7 or above. A subset of the final feature datasets was created from compounds identified at MSI level 1 and level 2 (Dataset 2). These datasets were processed in MetaboAnalyst (see Mass spectrometry analysis section, above) to generate heat maps, perform pathway analysis (see Pathway analysis section, below), and perform ANOVA analysis between strains exometabolite abundances.

All remaining unidentified compounds with MS/MS data were analyzed with CSI:Finger ID and assigned MSI level 3. This method provides the putative chemical ontology of a compound. The top CSI:Finger ID match was used for each compound. Then, InChI keys from all MSI levels were used to perform a chemical ontology analysis

using ClassyFire version 1.0. SDF files from ClassfyFire were exported from each analysis to extract both Class level and Direct Parent level ontologies. These data were then exported to R for data visualization.

RNA-Seq

RNA sample prep, sequencing, and QC

At Michigan State, RNA was extracted using the E.Z.N.A. Bacterial RNA kit (Omega Bio-tek, Inc.). An in-tube DNase I (Ambion, Inc AM2222, 2U) digestion was performed to remove DNA from RNA samples. RNA samples were purified and concentrated using the Qiagen RNAeasy MinElute Clean up Kit (Qiagen, Inc). Ten random samples were chosen to assess RNA integrity on an Agilent 2100 Bioanalyzer.

The following methods were according to DOE JGI standard operating protocols and performed at the DOE JGI facility. RNA samples were shipped from Michigan State to DOE JGI overnight on dry ice. RNA samples were placed into 4, 96-well plates- 1 plate for each species containing all stationary phase time points and 1 plate containing exponential phase time points. Plate-based RNA sample prep, including the Ribo-Zero rRNA Removal Kit (Illumina, for Bacteria) and the TruSeq Stranded Total RNA HT sample prep kit, was performed on the PerkinElmer Sciclone NGS robotic liquid handling system with the following conditions: total RNA starting material of 100 ng per sample and 10 cycles of PCR for library amplification. The prepared libraries were quantified using KAPA Biosystem's next-generation sequencing library qPCR kit and run on a Roche LightCycler 480 real-time PCR instrument. The quantified libraries were then prepared for sequencing on the Illumina HiSeq sequencing platform utilizing a TruSeq Rapid paired-end cluster kit, v4. Sequencing of the flowcell was performed on

the Illumina HiSeq2500 sequencer using HiSeq TruSeq SBS sequencing kits, v4, following a 2x100nt indexed run.

Read preprocessing and filtering

BBDuk (56) was used on raw fastq files to filter contaminants and trim both adaptor sequence and right quality trim reads where quality dropped to 0. Using BBDuk, raw reads were evaluated for artifact sequences by kmer matching (kmer=25), allowing 1 mismatch and detected artifacts were trimmed from the 3' end of the reads. BBDuk was used to remove reads that contained 1 or more 'N' bases, had an average quality score across the read less than 10 or had a minimum length <= 51 bp or 33% of the full read length. Reads mapped with BBMap (56) to masked human, cat, dog and mouse references at 93% identity were removed. Reads aligned to common microbial contaminants were also removed. Ribosomal RNA reads were also removed.

Pseudo-alignment and counting

The reads from each library were pseudo-aligned to the transcriptome of each strain with kallisto (57). Raw counts from each library were combined into gene count matrix for each strain. The gene count matrix was used for downstream analyses.

Transcriptomics

RNA quality filtering and differential gene expression (DGE) analysis

Count matrices for each strain were quality filtered in two steps prior to DGE: genes

containing 0 counts in all samples were removed and genes with a count ≤ 10 in more

than 90% of samples were removed. DGE was performed in DESeq2 version 1.22.1

(58). We tested for differential gene expression by evaluating genes that changed at

any time point (FDR < 0.01). Genes with differential expression were then evaluated for log₂ fold changes >1. Specifically, we focused on genes involved in transport (see Transporter analysis section, below). *Defining expression minimums*

A cumulative abundance plot was generated for each strain by organizing locus IDs from low transcript counts to high transcript counts and plotting the % of total transcripts against the % of total read counts (59, 60). The 25th quantile was calculated to obtain the transcript count value that defined a low expression minimum. That is, all genes with transcript counts above this minimum were considered to be expressed in the cell, regardless of longitudinal differential expression.

Transporter analysis

TransportDB 2.0 (http://www.membranetransport.org/transportDB2/index.html)
was used to annotate transporters in each strain (61). Annotated transporters were then evaluated to determine differential expression or expression above the low expression minimum.

KEGG pathway analysis

We extracted log₂ fold change (LFC) values from transcripts in each strain from DESeq analysis. Log₂ fold change were obtained by comparing each stationary phase time point to the exponential time point 1 (12.5 h). We then mapped longitudinal LFCs onto KEGG pathways for each strain using the pathview package in R. First, K numbers were assigned to genes for both *C. violaceum* and *P. syringae* using BlastKOALA (version 2.2). K numbers were not assigned to *B. thailandensis* because KEGG identifiers were available. KEGG identifiers for *B. thailandensis* and K numbers

assigned to *C. violaceum* and *P. syringae* were used to map longitudinal LFCs onto KEGG pathways. Pathways of interest were curated and manually edited in Inkscape (verision 0.92.4) using a colorblind palette.

Annotation of biosynthetic gene clusters (BSGC)

BSGC were annotated using antismash bacterial version 5.0 (62). Annotated genome files for each strain were submitted to the online server. Default parameters included a relaxed detection strictness and extra features such as KnownClusterBlast, SubClusterBlast, and ActiveSiteFinder.

Code availability

Computing code and workflows and datasets are available at

https://github.com/ShadeLab/Paper_Chodkowski_MonocultureExometabolites_2020. R packages used during computing analyses included vegan (63), ggplot2 (64),

VennDiagram (65), RVAideMemoire (66), patchwork (67), DESeq2 (58), pathview (68),

KEGGREST (69), and helper functions (70–73).

Data availability

Genomes for *B. thailandensis*, *C. violaceum*, and *P. syringae* are available at JGI Genome Portal under project IDs 1133672, 1133669, and 1133674, respectively. An improved annotated draft genome of *C. violaceum* is available under NCBI BioProject number PRJNA402426 (Genbank Accession ID: PKBZ00000000). Re-sequencing efforts for *B. thailandensis* and *P. syringae* are under NCBI BioProject numbers PRJNA402425 and PRJNA402424, respectively. Metabolomics data and

- transcriptomics data are also available at JGI Genome Portal (74) under JGI Proposal
- 713 ID 502921. MZmine XML parameter files for all analyses can be viewed and
- downloaded from GitHub (<u>Dataset 7</u>). Large data files (e.g. MZmine project files) are
- available upon request. Other datasets are also available on GitHub (Datasets).

716

717 References

718

- 719 1. Lewis DL, Gattie DK. 1991. Ecology of quiescent microbes, ASM News 57:27–32.
- 720 2. Cole JJ. 1999. Aquatic microbiology for ecosystem scientists: New and recycled paradigms in ecological microbiology. Ecosystems 2:215–225.
- 3. Blazewicz SJ, Barnard RL, Daly RA, Firestone MK. 2013. Evaluating rRNA as an indicator of microbial activity in environmental communities: Limitations and uses. ISME J 7:2061–2068.
- Schimel JP. 2018. Life in dry soils: Effects of drought on soil microbial communities and processes.
 Annu Rev Ecol Evol Syst 49:409–432.
- 5. Göransson H, Godbold DL, Jones DL, Rousk J. 2013. Bacterial growth and respiration responses upon rewetting dry forest soils: Impact of drought-legacy. Soil Biol Biochem 57:477–486.
- 728 6. Meisner A, Leizeaga A, Rousk J, Bååth E. 2017. Partial drying accelerates bacterial growth recovery to rewetting. Soil Biol Biochem 112:269–276.
- 730 7. Ni BJ, Fang F, Rittmann BE, Yu HQ. 2009. Modeling microbial products in activated sludge under feast-famine conditions. Environ Sci Technol 43:2489–2497.
- 732 8. Chiesa SC, Irvine RL, Manning JF. 1985. Feast/famine growth environments and activated sludge population selection. Biotechnol Bioeng 27:562–568.
- 734 9. Fetissov SO. 2017. Role of the gut microbiota in host appetite control: Bacterial growth to animal feeding behaviour. Nat Rev Endocrinol 13:11–25.
- Breton J, Tennoune N, Lucas N, Francois M, Legrand R, Jacquemot J, Goichon A, Guérin C, Peltier
 J, Pestel-Caron M, Chan P, Vaudry D, Do Rego JC, Liénard F, Pénicaud L, Fioramonti X, Ebenezer
 IS, Hökfelt T, Déchelotte P, Fetissov SO. 2016. Gut commensal E. coli proteins activate host
 satiety pathways following nutrient-induced bacterial growth. Cell Metab 23:324–334.
- 740 11. Kolter R, Siegele DA, Tormo A. 1993. The Stationary Phase of The Bacterial Life Cycle. Annu Rev 741 Microbiol 47:855–874.
- 742 12. De Nobili M, Contin M, Mondini C, Brookes PC. 2001. Soil microbial biomass is triggered into activity by trace amounts of substrate. Soil Biol Biochem 33:1163–1170.
- 5wieciło A, Zych-Wezyk I. 2013. Bacterial stress response as an adaptation to life in a soil
 environment. Polish J Environ Stud 22:1577–1587.

- Jaishankar J, Srivastava P. 2017. Molecular basis of stationary phase survival and applications.
 Front Microbiol 8:2000.
- 748 15. Navarro Llorens JM, Tormo A, Martínez-García E. 2010. Stationary phase in gram-negative bacteria. FEMS Microbiol Rev 34:476–95.
- 750 16. Bergkessel M, Basta DW, Newman DK. 2016. The physiology of growth arrest: Uniting molecular and environmental microbiology. Nat Rev Microbiol 14:549–562.
- 17. Lever MA, Rogers KL, Lloyd KG, Overmann J, Schink B, Thauer RK, Hoehler TM, Jørgensen BB.
- 753 2015. Life under extreme energy limitation: A synthesis of laboratory- and field-based investigations. FEMS Microbiol Rev 39:688–728.
- 755 18. Gefen O, Fridman O, Ronin I, Balaban NQ. 2014. Direct observation of single stationary-phase 756 bacteria reveals a surprisingly long period of constant protein production activity. Proc Natl Acad 757 Sci 111:556–561.
- 758 19. Rinas U, Hellmutii K, Kang R, Seeger A, Schlieker H. 1995. Entry of Escherichia coli into stationary 759 phase is indicated by endogenous and exogenous accumulation of nucleobases. Appl Environ 760 Microbiol 61:4147–51.
- 761 20. Brauer MJ, Yuan J, Bennett BD, Lu W, Kimball E, Botstein D, Rabinowitz JD. 2006. Conservation of 762 the metabolomic response to starvation across two divergent microbes. Proc Natl Acad Sci U S A 763 103:19302–19307.
- Link H, Fuhrer T, Gerosa L, Zamboni N, Sauer U. 2015. Real-time metabolome profiling of the metabolic switch between starvation and growth. Nat Methods 12:1091.
- Silva LP, Northen TR. 2015. Exometabolomics and MSI: Deconstructing how cells interact to transform their small molecule environment. Curr Opin Biotechnol 34:209–216.
- Kell DB, Brown M, Davey HM, Dunn WB, Spasic I, Oliver SG. 2005. Metabolic footprinting and systems biology: The medium is the message. Nat Rev Microbiol 3:557–65.
- 770 24. Phelan V V, Liu W-T, Pogliano K, Dorrestein PC. 2011. Microbial metabolic exchange--the chemotype-to-phenotype link. Nat Chem Biol 8:26–35.
- 772 25. Pacheco AR, Moel M, Segrè D. 2019. Costless metabolic secretions as drivers of interspecies interactions in microbial ecosystems. Nat Commun 10:103.
- 774 26. Ren JL, Zhang AH, Kong L, Wang XJ. 2018. Advances in mass spectrometry-based metabolomics 775 for investigation of metabolites. RSC Adv 8:22335–22350.
- 776 27. Chandler JR, Heilmann S, Mittler JE, Greenberg EP. 2012. Acyl-homoserine lactone-dependent 777 eavesdropping promotes competition in a laboratory co-culture model. ISME J 6:2219–28.
- Chodkowski JL, Shade A. 2017. A Synthetic Community System for Probing Microbial Interactions
 Driven by Exometabolites. mSystems 2:e00129-17.
- 780 29. Duerkop BA, Varga J, Chandler JR, Peterson SB, Herman JP, Churchill MEA, Parsek MR, Nierman
 781 WC, Greenberg EP. 2009. Quorum-sensing control of antibiotic synthesis in Burkholderia
 782 thailandensis. J Bacteriol 191:3909–3918.
- 783 30. Jones AM, Lindow SE, Wildermuth MC. 2007. Salicylic acid, yersiniabactin, and pyoverdin

- production by the model phytopathogen Pseudomonas syringae pv. tomato DC3000: synthesis, regulation, and impact on tomato and Arabidopsis host plants. J Bacteriol 189:6773–86.
- McClean KH, Winson MK, Fish L, Taylor A, Chhabra SR, Camara M, Daykin M, Lamb JH, Swift S,
 Bycroft BW, Stewart GS, Williams P. 1997. Quorum sensing and Chromobacterium violaceum:
 Exploitation of violacein production and inhibition for the detection of N-acylhomoserine
 lactones. Microbiology 143:3703-3711.
- 790 32. Kothari V, Sharma S, Padia D. 2017. Recent research advances on Chromobacterium violaceum. 791 Asian Pac J Trop Med 10:744–752.
- Gude S, Pherribo GJ, Taga ME. 2020. Emergence of Metabolite Provisioning as a By-Product of
 Evolved Biological Functions. mSystems 5:e00259-20.
- 794 34. Schink SJ, Biselli E, Ammar C, Gerland U. 2019. Death Rate of E. coli during Starvation Is Set by Maintenance Cost and Biomass Recycling. Cell Syst 9:64–73.
- 796 35. Nyström T. 2004. Stationary-Phase Physiology. Annu Rev Microbiol 58:161–81.
- Lewis RA, Bignell CR, Zeng W, Jones AC, Thomas CM. 2002. Chromosome loss from par mutants
 of Pseudomonas putida depends on growth medium and phase of growth. Microbiology
 148:537–548.
- 800 37. Shimaya T, Okura R, Wakamoto Y, Takeuchi KA. 2020. Scale invariance during bacterial reductive 801 division observed by an extensive microperfusion system. bioRxiv doi: 802 10.1101/2020.06.25.171710.
- 803 38. Piir K, Paier A, Liiv A, Tenson T, Maiväli Ü. 2011. Ribosome degradation in growing bacteria. 804 EMBO Rep 12:458–462.
- 805 39. Paczia N, Nilgen A, Lehmann T, Gätgens J, Wiechert W, Noack S. 2012. Extensive exometabolome 806 analysis reveals extended overflow metabolism in various microorganisms. Microb Cell Fact 807 11:122.
- Kandler JR, Truong TT, Silva PM, Seyedsayamdost MR, Carr G, Radey M, Jacobs MA, Sims EH,
 Clardy J, Greenberg EP. 2012. Bactobolin resistance is conferred by mutations in the L2 ribosomal protein. MBio 3:e00499-12.
- 811 41. Birch LC. 1957. The meanings of competition. Am Nat 91:5–18.
- 812 42. Miller RS. 1967. Pattern and Process in Competition. Adv Ecol Res 4:1–74.
- Hibbing ME, Fuqua C, Parsek MR, Peterson SB. 2010. Bacterial competition: surviving and thriving in the microbial jungle. Nat Rev Microbiol 8:15–25.
- Abe T, Kobayashi K, Kawamura S, Sakaguchi T, Shiiba K, Kobayashi M. 2019. Dipeptide synthesis
 by internal adenylation domains of a multidomain enzyme involved in nonribosomal peptide
 synthesis. J Gen Appl Microbiol 65:1–10.
- Kano S, Suzuki S, Hara R, Kino K. 2019. Synthesis of D-Amino Acid-Containing Dipeptides Using
 the Adenylation Domains of Nonribosomal Peptide Synthesis. Appl Environ Microbiol
 85:e00120-19.
- 46. Waters CM, Bassler BL. 2005. QUORUM SENSING: Cell-to-Cell Communication in Bacteria. Annu

- 822 Rev Cell Dev Biol 21:319–346.
- 823 47. Blaženović I, Kind T, Sa MR, Ji J, Vaniya A, Wancewicz B, Roberts BS, Torbašinović H, Lee T, Mehta 824 SS, Showalter MR, Song H, Kwok J, Jahn D, Kim J, Fiehn O. 2019. Structure Annotation of All Mass 825 Spectra in Untargeted Metabolomics. Anal Chem 91:2155–2162.
- 48. Goo E, Majerczyk CD, An JH, Chandler JR, Seo Y-S, Ham H, Lim JY, Kim H, Lee B, Jang MS,
 Greenberg EP, Hwang I. 2012. Bacterial quorum sensing, cooperativity, and anticipation of
 stationary-phase stress. Proc Natl Acad Sci U S A 109:19775–80.
- 49. Goo E, Kang Y, Lim JY, Ham H, Hwang I. 2017. Lethal consequences of overcoming metabolic restrictions imposed on a cooperative bacterial population. MBio 8:e00042-17.
- Sass AM, Schmerk C, Agnoli K, Norville PJ, Eberl L, Valvano MA, Mahenthiralingam E. 2013. The unexpected discovery of a novel low-oxygen-activated locus for the anoxic persistence of Burkholderia cenocepacia. ISME J 7:1568–1581.
- 834 51. Banerjee D, Raghunathan A. 2019. Constraints-based analysis identifies NAD + recycling through 835 metabolic reprogramming in antibiotic resistant chromobacterium violaceum. PLoS One 836 14:e0210008.
- 837 52. Pluskal T, Castillo S, Villar-Briones A, Orešič M. 2010. MZmine 2: Modular framework for 838 processing, visualizing, and analyzing mass spectrometry-based molecular profile data. BMC 839 Bioinformatics 11:395.
- S40 S3. Chong J, Soufan O, Li C, Caraus I, Li S, Bourque G, Wishart DS, Xia J. 2018. MetaboAnalyst 4.0:
 Towards more transparent and integrative metabolomics analysis. Nucleic Acids Res 46:W486–W494.
- Schymanski EL, Jeon J, Gulde R, Fenner K, Ruff M, Singer HP, Hollender J. 2014. Identifying small
 molecules via high resolution mass spectrometry: Communicating confidence. Environ Sci
 Technol 48:2097–2098.
- 846 55. Wang M, Carver JJ, Phelan V V., Sanchez LM, Garg N, Peng Y, Nguyen DD, Watrous J, Kapono CA, 847 Luzzatto-Knaan T, Porto C, Bouslimani A, Melnik A V., Meehan MJ, Liu WT, Crüsemann M, 848 Boudreau PD, Esquenazi E, Sandoval-Calderón M, Kersten RD, Pace LA, Quinn RA, Duncan KR, Hsu 849 CC, Floros DJ, Gavilan RG, Kleigrewe K, Northen T, Dutton RJ, Parrot D, Carlson EE, Aigle B, 850 Michelsen CF, Jelsbak L, Sohlenkamp C, Pevzner P, Edlund A, McLean J, Piel J, Murphy BT, 851 Gerwick L, Liaw CC, Yang YL, Humpf HU, Maansson M, Keyzers RA, Sims AC, Johnson AR, 852 Sidebottom AM, Sedio BE, Klitgaard A, Larson CB, Boya CAP, Torres-Mendoza D, Gonzalez DJ, 853 Silva DB, Margues LM, Demargue DP, Pociute E, O'Neill EC, Briand E, Helfrich EJN, Granatosky EA, 854 Glukhov E, Ryffel F, Houson H, Mohimani H, Kharbush JJ, Zeng Y, Vorholt JA, Kurita KL, Charusanti 855 P, McPhail KL, Nielsen KF, Vuong L, Elfeki M, Traxler MF, Engene N, Koyama N, Vining OB, Baric R, 856 Silva RR, Mascuch SJ, Tomasi S, Jenkins S, Macherla V, Hoffman T, Agarwal V, Williams PG, Dai J, 857 Neupane R, Gurr J, Rodríguez AMC, Lamsa A, Zhang C, Dorrestein K, Duggan BM, Almaliti J, Allard 858 PM, Phapale P, Nothias LF, Alexandrov T, Litaudon M, Wolfender JL, Kyle JE, Metz TO, Peryea T, 859 Nguyen DT, VanLeer D, Shinn P, Jadhav A, Müller R, Waters KM, Shi W, Liu X, Zhang L, Knight R, 860 Jensen PR, Palsson B, Pogliano K, Linington RG, Gutiérrez M, Lopes NP, Gerwick WH, Moore BS, 861 Dorrestein PC, Bandeira N. 2016. Sharing and community curation of mass spectrometry data
- with Global Natural Products Social Molecular Networking. Nat Biotechnol 34:828–837.
- 863 56. Bushnell B. 2015. BBMap (version 37.75). Available at https://sourceforge.net/projects/bbmap/.

- 864 57. Bray NL, Pimentel H, Melsted P, Pachter L. 2016. Near-optimal probabilistic RNA-seq quantification. Nat Biotechnol 34:525–527.
- Love MI, Huber W, Anders S. 2014. Moderated estimation of fold change and dispersion for RNAseq data with DESeq2. Genome Biol 15:550.
- 868 59. Bullard JH, Purdom E, Hansen KD, Dudoit S. 2010. Evaluation of statistical methods for normalization and differential expression in mRNA-Seq experiments. BMC Bioinformatics 11:94.
- Raithel S, Johnson L, Galliart M, Brown S, Shelton J, Herndon N, Bello NM. 2016. Inferential
 considerations for low-count RNA-seq transcripts: A case study on the dominant prairie grass
 Andropogon gerardii. BMC Genomics 17:140.
- 873 61. Elbourne LDH, Tetu SG, Hassan KA, Paulsen IT. 2017. TransportDB 2.0: A database for exploring membrane transporters in sequenced genomes from all domains of life. Nucleic Acids Res 45:D320–D324.
- 876 62. Blin K, Shaw S, Steinke K, Villebro R, Ziemert N, Lee SY, Medema MH, Weber T. 2019. AntiSMASH
 877 5.0: Updates to the secondary metabolite genome mining pipeline. Nucleic Acids Res 47:W81–
 878 W87.
- 879 63. Oksanen J, Blanchet FG, Friendly M, Kindt R, Legendre P, McGlinn D, Minchin PR, O'Hara RB, 880 Simpson GL, Solymos P, Stevens MHH, Szoecs E, Wagner H. 2019. vegan: Community Ecology 881 Package. R package version 2.5-4.
- 882 64. Wickham H. 2009. Ggplot2Elegant Graphics for Data Analysis.
- 883 65. Chen H. 2018. VennDiagram: Generate High-Resolution Venn and Euler Plots. R package version 1.6.20.
- 885 66. Maxime Herve. 2020. RVAideMemoire: Testing and Plotting Procedures for Biostatistics. R Packag version 09-77.
- 887 67. Pedersen TL. 2020. patchwork: The Composer of Plots.

900

- 888 68. Luo W, Brouwer C. 2013. Pathview: an R/Bioconductor package for pathway-based data integration and visualization. Bioinformatics2013/06/04. 29:1830–1831.
- 890 69. Tenenbaum D. 2018. KEGGREST: Client-side REST access to KEGG. R package version 1.22.0.
- Wickham H. 2019. stringr: Simple, Consistent Wrappers for Common String Operations. R package version 1.4.0.
- Wickham H, François R, Henry L, Müller K. 2019. dplyr: A Grammar of Data Manipulation. R package version 0.8.3.
- 895 72. Wickham H. 2011. The split-apply-combine strategy for data analysis. J Stat Softw 40:1–29.
- 896 73. Wickham H. 2007. Reshaping data with the reshape package. J Stat Softw 21:1–20.
- Nordberg H, Cantor M, Dusheyko S, Hua S, Poliakov A, Shabalov I, Smirnova T, Grigoriev I V.,

 Dubchak I. 2014. The genome portal of the Department of Energy Joint Genome Institute: 2014

 updates. Nucleic Acids Res 42:D26-31.

901 Author contributions statement 902 J.C. and A.S. conceived of and designed the study. J.C. performed the research and 903 analyses. J.C. and A.S. wrote the manuscript. 904 Acknowledgments 905 This material is based upon work supported by the National Science Foundation under 906 907 Grant DEB #1749544, by Michigan State University. In addition, metabolite analysis and transcript sequencing were provided by a DOE-JGI Community Science Program award 908 909 (Proposal ID 502921). The work conducted by the U.S. Department of Energy Joint 910 Genome Institute, a DOE Office of Science User Facility, is supported under Contract 911 No. DE-AC02-05CH11231. J.C. was supported by the Eleanor L. Gilmore Fellowship from the Department of Microbiology and Molecular Genetics. We thank Katherine B. 912 913 Louie and Benjamin P. Bowen for support in mass spectral analysis. 914 Additional information 915 Competing interest statements 916 917 The authors declare no competing interests

Figure legends

Figure 1. Quantification of all features that fit criteria for released in all strains across all polarity/ionization modes.

Figure 2. Exometabolite profiles differ by strain and time. PCoA plots for polar positive (A), polar negative (B), nonpolar positive (C), nonpolar negative (D), and combined polar positive + polar negative exometabolites (accounting for 72-77% of released exometabolites per strain) for *B. thailandensis* (E), *C. violaceum* (F), and *P. syringae* (G). Each point represents the exometabolite profile (relative contributions assessed by peak area) for a particular strain at a particular time point. Features were normalized by an internal standard (ITSD) reference feature and cube root transformed. Bray-Curtis distance metric was used to calculate dissimilarities between exometabolite profiles. Strain is indicated by shape (*B. thailandensis* (●), *C. violaceum* (▲), *P. syringae* (■)) and timepoint is indicated by a color gradient. Error bars are 1 standard deviation around the mean axis scores of n = 2 to 4 replicates destructively sampled from the same strain/time point condition.

Figure 3. Released exometabolites and their temporal dynamics. A heat map of all released exometabolites is shown for A) polar positive, B) polar negative, C) nonpolar positive, and D) nonpolar negative modes, where samples are columns are exometabolites are in rows. Each sample is the average of independent time point replicates (n = 2 to 4). Euclidean distance was calculated from Z-scored mass spectral

profiles (containing peak areas). Prior to Z-scoring, features were normalized by an internal standard (ITSD) reference feature and cube root transformed. Features were clustered by Ward's method.

Figure 4. Released and identified exometabolites and their temporal dynamics. A heat map of identified exometabolites in polar positive mode is shown, where samples are columns are exometabolites are in rows. Each sample is the average of independent time point replicates (n = 3 or 4). Euclidean distance was calculated from Z-scored mass spectral profiles (containing peak areas). Prior to Z-scoring, features were normalized by an internal standard (ITSD) reference feature and cube root transformed. Features were clustered by Ward's method.

Figure 5. Chemical ontologies at different MSI levels. ClassyFire was used to categorize identified (MSI level 1 and level 2) and *in silico* predicted MS/MS data (MSI level 3) at the a) class and b) direct parent levels. Identification confidence 1,2, and 3 refers to Metabolomics Standards Initiative (MSI) identification levels 1, 2, and 3, respectively. The top ten chemical ontologies are provided for each classification level. Chemical ontologies for panel A: 1) Azoles, 2) Benzene and substituted derivatives, 3) Carboxylic acids and derivatives, 4) Diazines, 5) Fatty Acyls, 6) Imidazopyrimidines, 7) Organonitrogen compounds, 8) Organooxygen compounds, 9) Purine nucleosides, 10) Pyridines and derivatives. Chemical ontologies for panel B: 1) Alpha amino acids, 2) Dipeptides, 3) Hydroxybenzoic acid derivatives, 4) Hydroxypyrimidines, 5) Medium-

chain fatty acids, 6) N-acyl-alpha amino acids, 7) N-acyl-alpha amino acids and derivatives, 8) Peptides, 9) Purine nucleosides, 10) 6-alkylaminopurines.

Figure 6. Distinctions and overlaps between the most abundant exometabolites in each strain. Exometabolites in bold passed criteria for released. Exometabolites in italics are isomers and could not be resolved to determine the exact identification.

Figure 7. Temporal changes in transcriptomics reveal re-routing of metabolism towards succinate production. Log₂-fold change (LFC) values were mapped onto pathways involved in succinate production for a) *B. thailandensis*, b) *C. violaceum*, and c) *P. syringae*. LFC values are represented by rectangles alongside each reaction in the pathway map. Each column represents the 5 stationary phase time points. Colors within each rectangle represent LFC (green-increased transcripts, red-decreased transcripts) compared to the exponential phase time point.

Table captions 978 **Table 1**. Bacterial strains used in this study. 979 980 Table 2: Summary of released exometabolites for each strain. Bt is B. thailandensis, Cv 981 is C. violaceum, and Ps is P. syringae. 982 983 **Table 3**: Summary of RNA-Seg results with focus on genes annotated as transporters. 984 Criteria included genes that were a) above the low expression minimum (LEM), b) 985 genes that were differentially expressed, and c) genes with a stationary phase time 986 point that had a log₂ fold change (LFC) > 1 compared to the exponential phase time 987 point. 988

Supplemental figure legends

Supplementary Figure S1. Counts of live (green) and dead (blue) cells throughout the time course. Cells were obtained from 5 wells in the transwell plate for 5 technical replicates/independent replicate at each time point. Syto9 and propidium iodide-stained cells were counted using flow cytometry.

Supplementary Figure S2. Released and identified exometabolites and their temporal dynamics. A heat map of identified exometabolites in polar negative mode is shown, where samples are columns and exometabolites are in rows. Each sample is the average of independent time point replicates (n = 3 or 4). Euclidean distance was calculated from Z-scored mass spectral profiles (containing peak areas). Prior to Z-scoring, features were normalized by an internal standard (ITSD) reference feature and cube root transformed. Features were clustered by Ward's method.

Supplementary Figure S3. Released and identified exometabolites and their temporal dynamics. A heat map of identified exometabolites in nonpolar positive mode is shown, where samples are columns and exometabolites are in rows. Each sample is the average of independent time point replicates (n = 2 to 4). Euclidean distance was calculated from Z-scored mass spectral profiles (containing peak areas). Prior to Z-scoring, features were normalized by an internal standard (ITSD) reference feature and cube root transformed. Features were clustered by Ward's method.

Supplementary Figure S4. Released and identified exometabolites and their temporal dynamics. A heat map of identified exometabolites in nonpolar negative mode is shown, where samples are columns and exometabolites are in rows. Each sample is the average of independent time point replicates (n = 2 to 4). Euclidean distance was calculated from Z-scored mass spectral profiles (containing peak areas). Prior to Z-scoring, features were normalized by an internal standard (ITSD) reference feature and cube root transformed. Features were clustered by Ward's method.

Supplemental table captions

Supplementary Table S1. Percent variation explained on the effect of strain, time, and their interaction on exometabolite profiles. Permanova revealed strain-specific differences in exometabolite composition (all $P \le 0.001$).

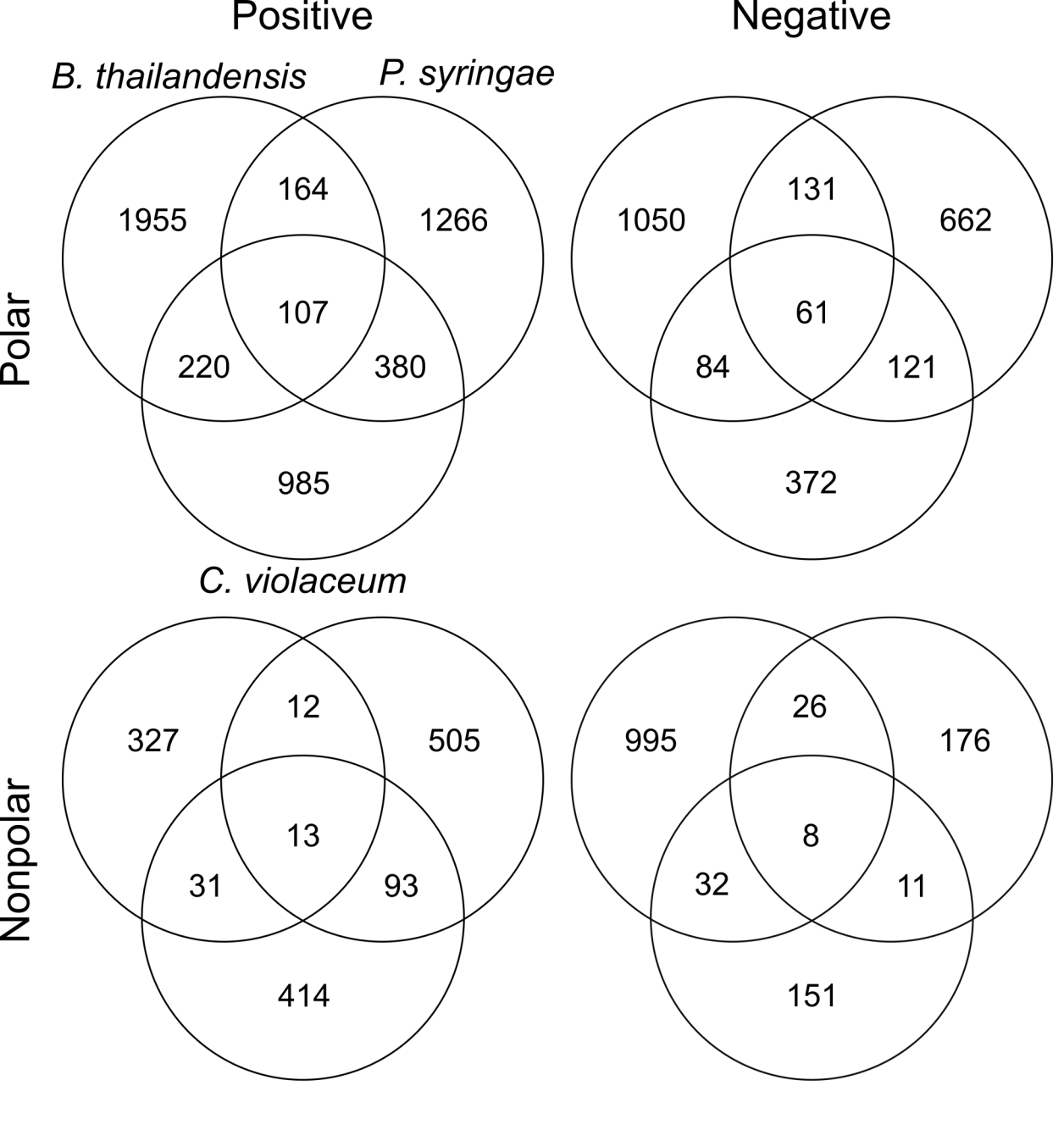
Supplementary Table S2. Summary of Protest analyses comparing exometabolite composition through time across independent replicates. Coordinates of the first two PCoA axes were used to perform Protest analyses. Ranges reflect separate Protest analyses performed for each polarity (polar/nonpolar) and ionization mode (positive/negative).

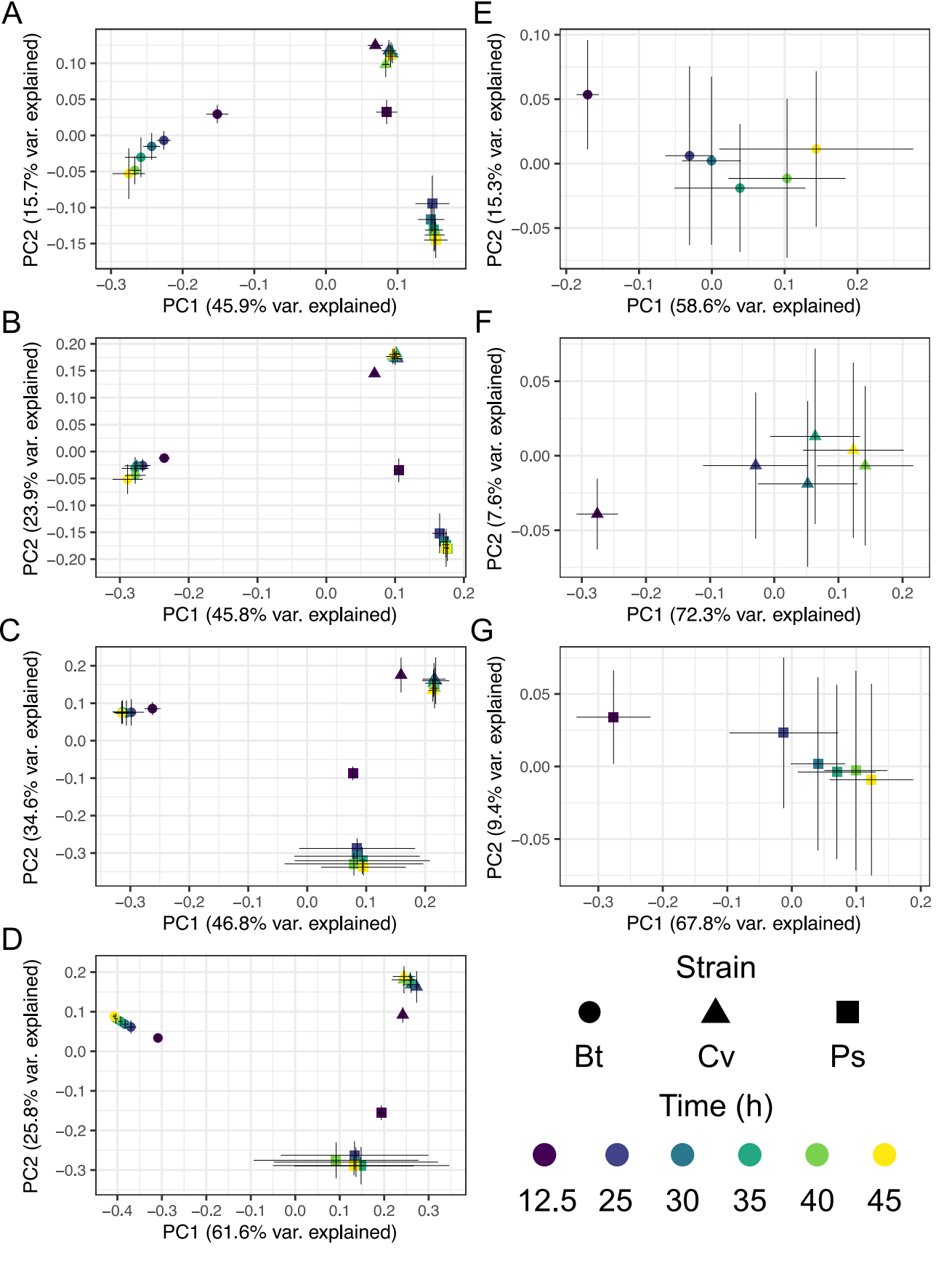
Supplementary Table S3. Average Bray-Curtis dissimilarity between group centroids when comparing each stationary phase time point to the initial, exponential phase time point (12.5 h). Ranges reflect separate analyses performed for each polarity (polar/nonpolar) and ionization mode (positive/negative).

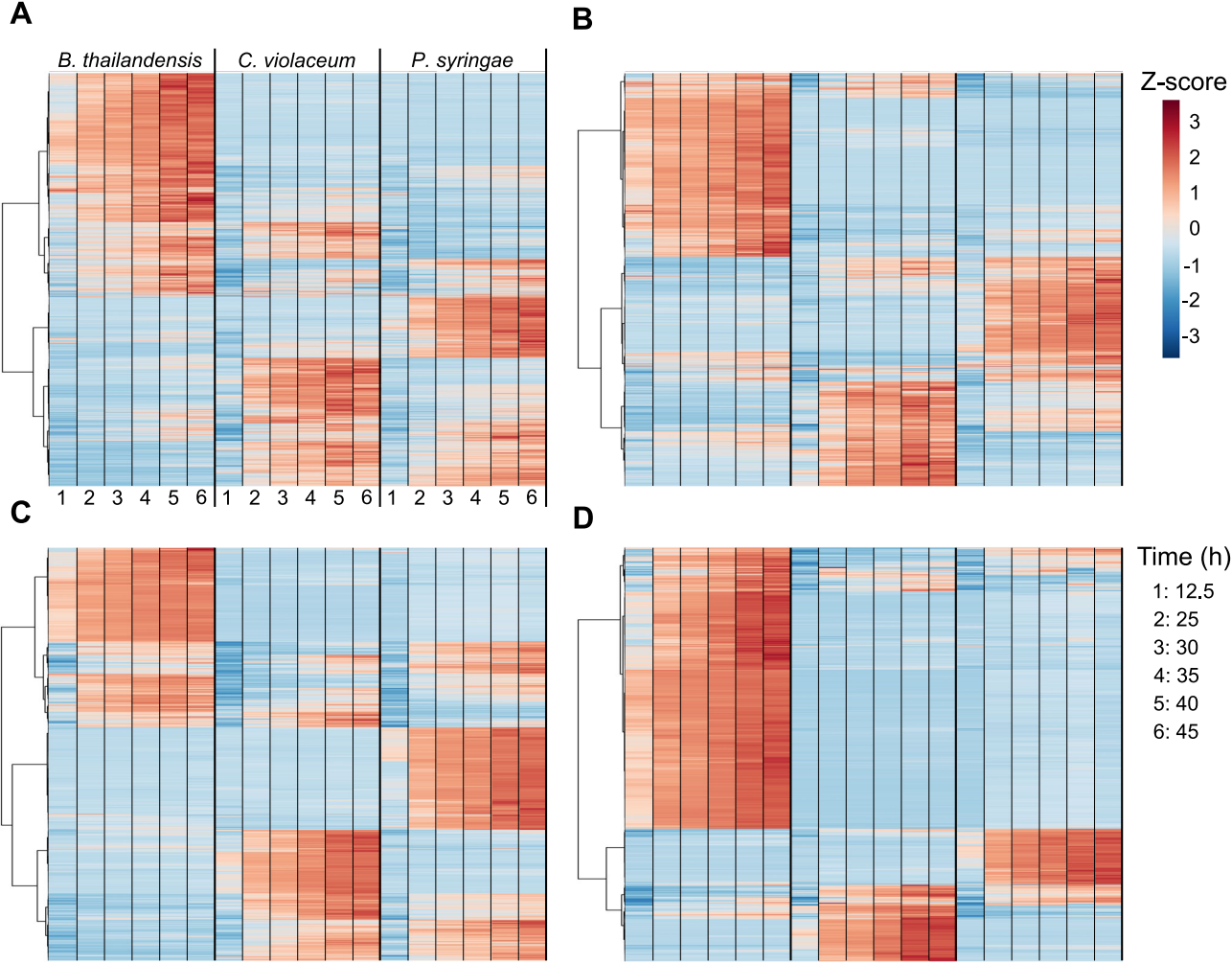
Supplementary Table S4. Average Bray-Curtis dissimilarity between group centroids when comparing time points in a step-wise manner. Ranges reflect separate analyses performed for each polarity (polar/nonpolar) and ionization mode (positive/negative).

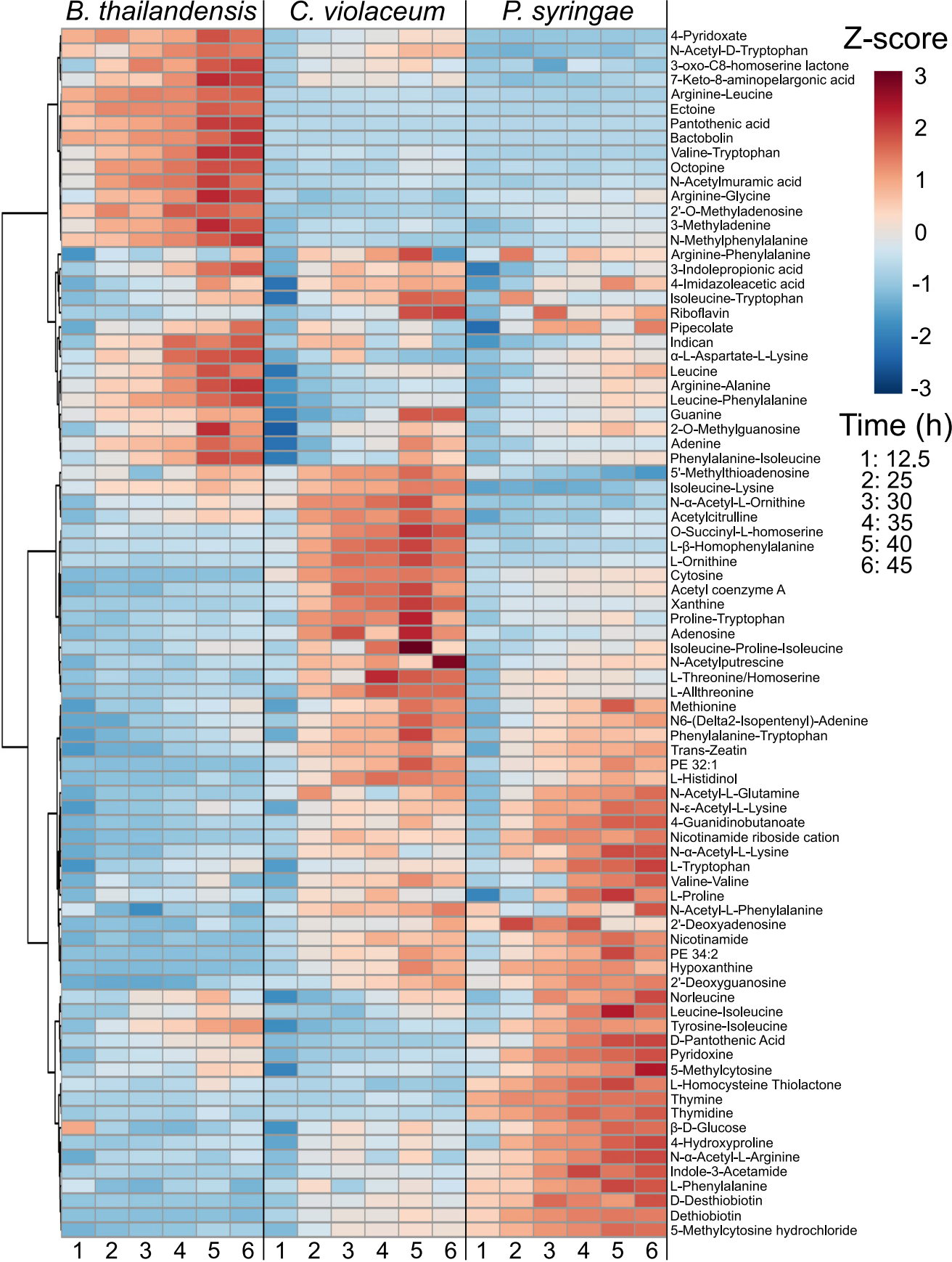
Supplementary Table S5. Repeated measures permanova performed on
independently replicated time series within each strain. *P* values are listed followed by
R2 values in parenthesis.

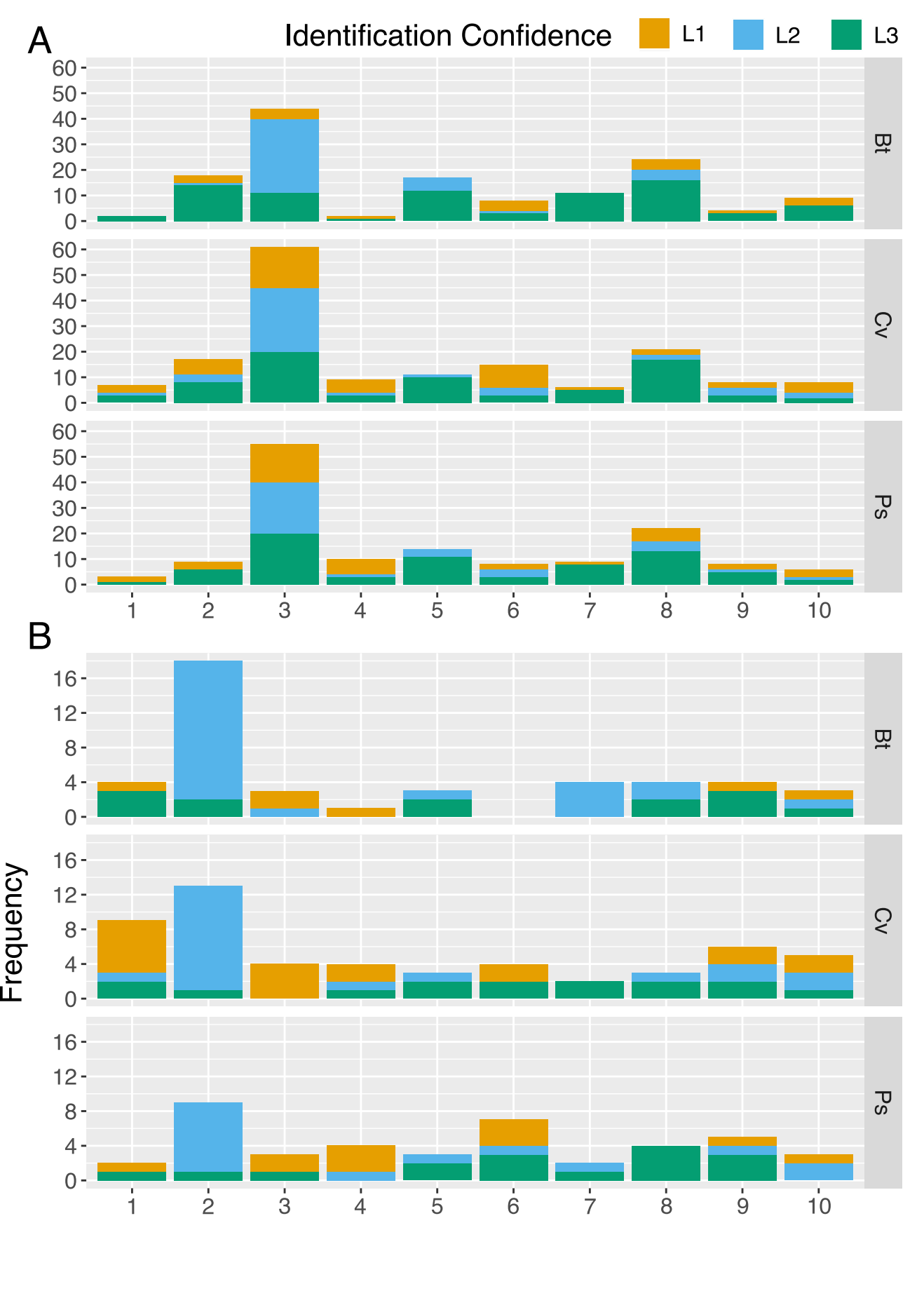
Supplementary Table S6. Q-values from pairwise adonis tests comparing all time
points within a strain. Ranges reflect separate analyses performed for each polarity
(polar/nonpolar) and ionization mode (positive/negative).

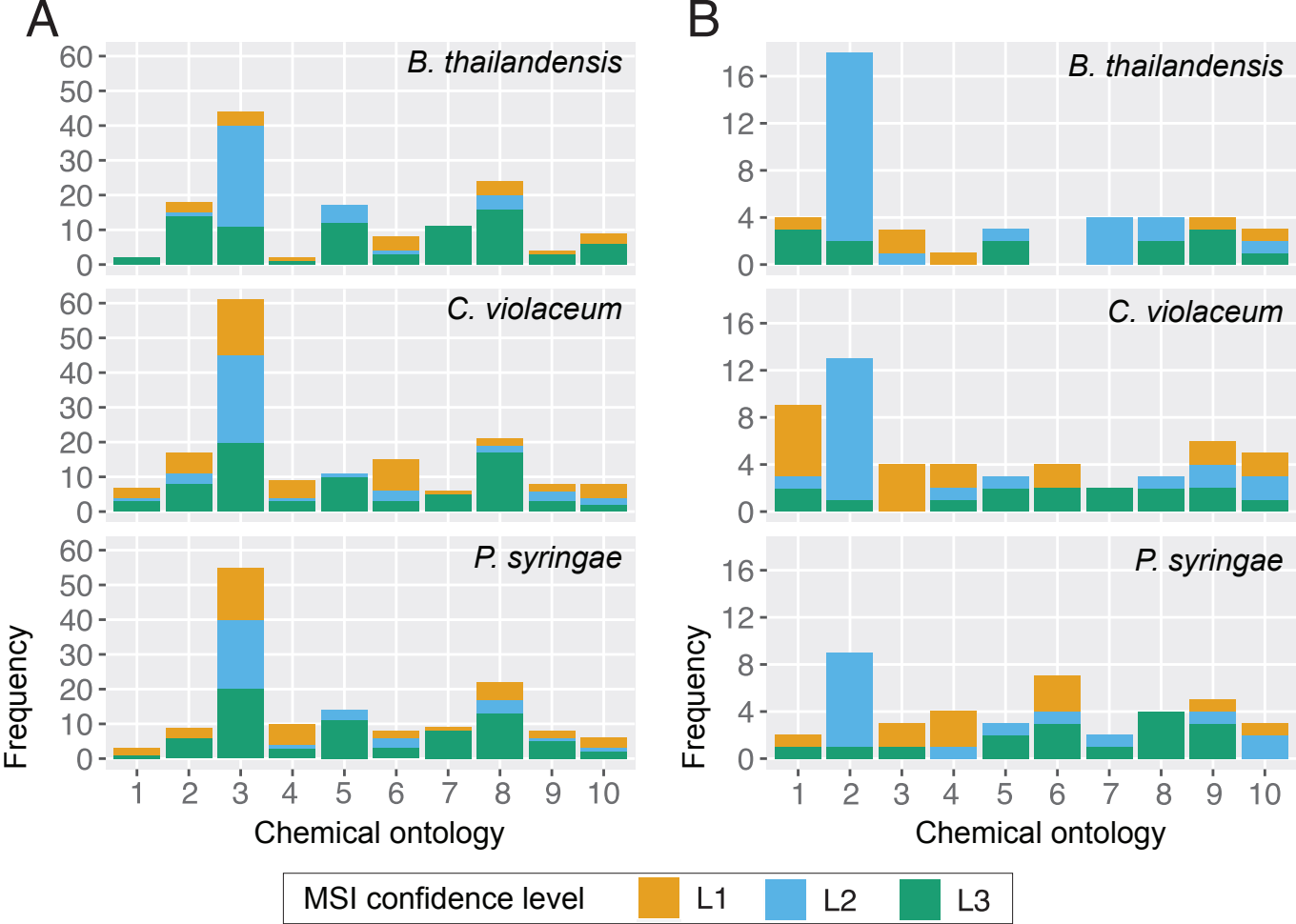


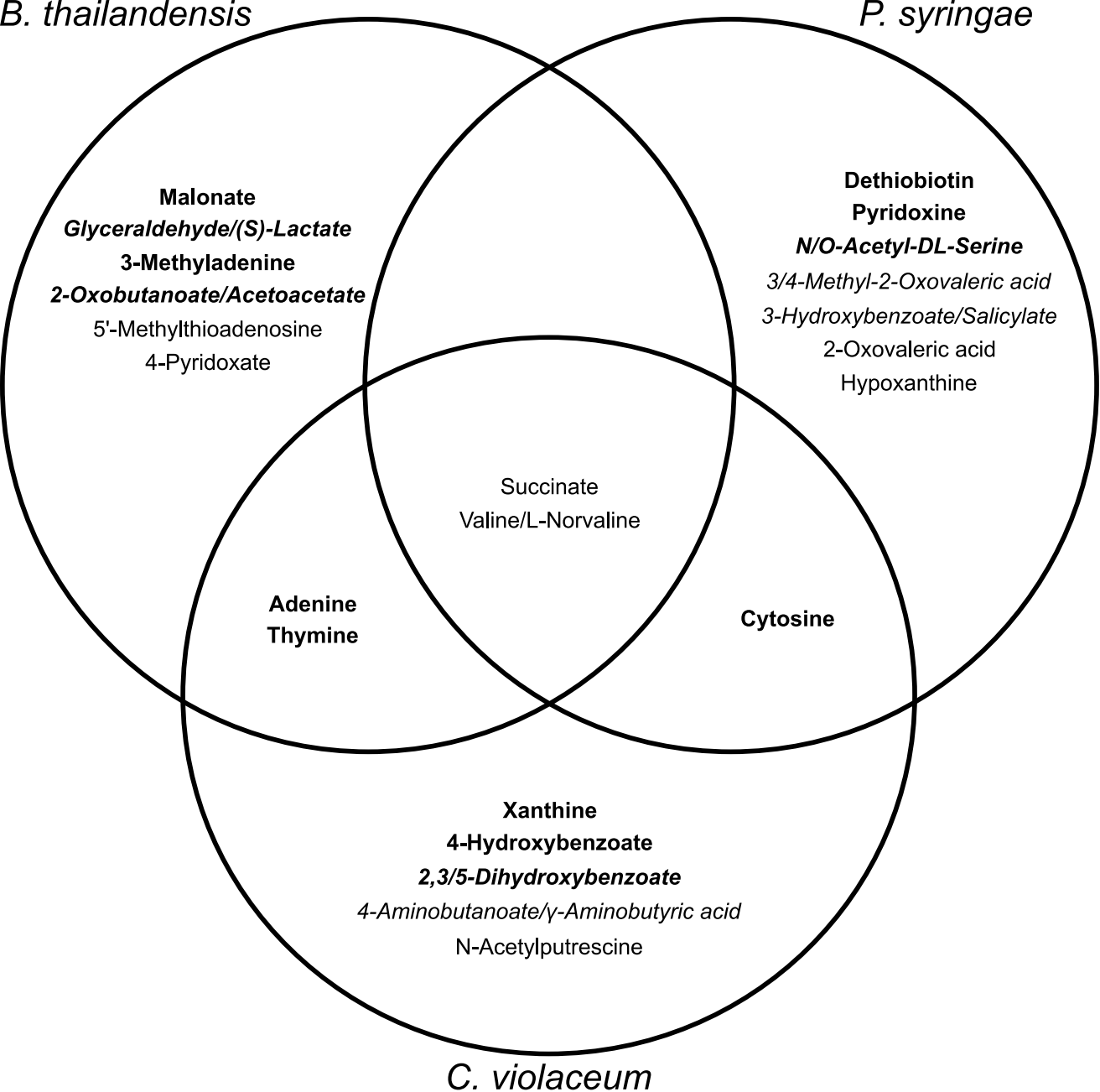












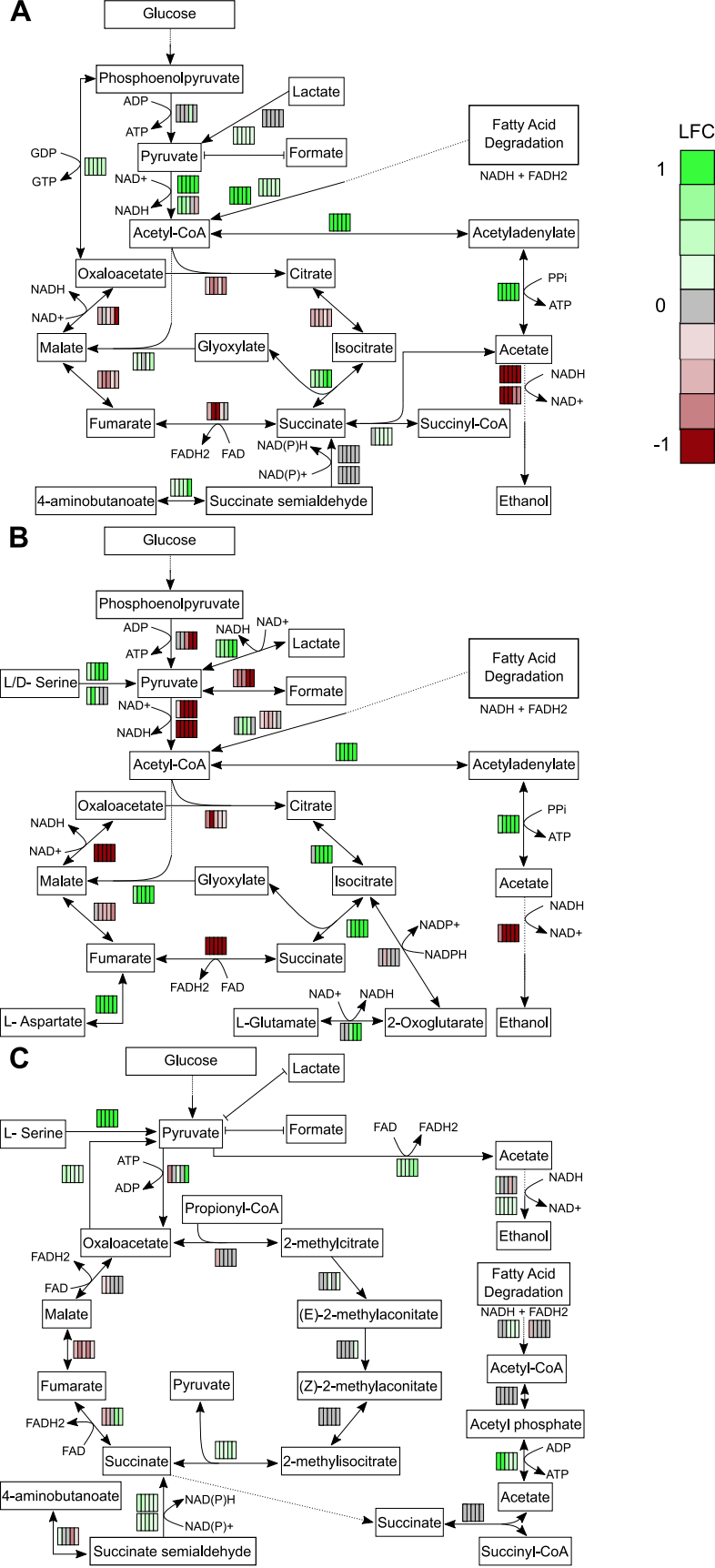
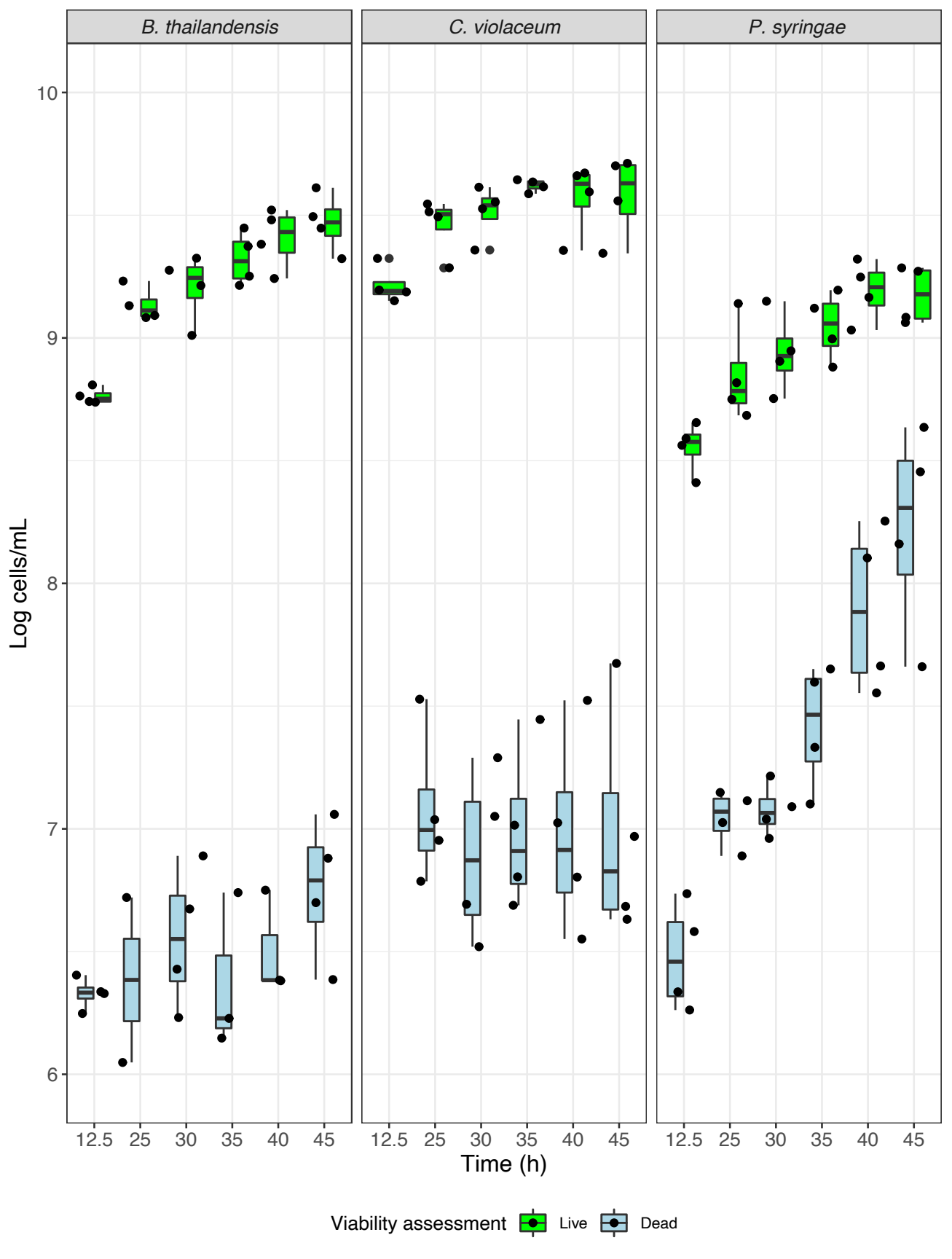


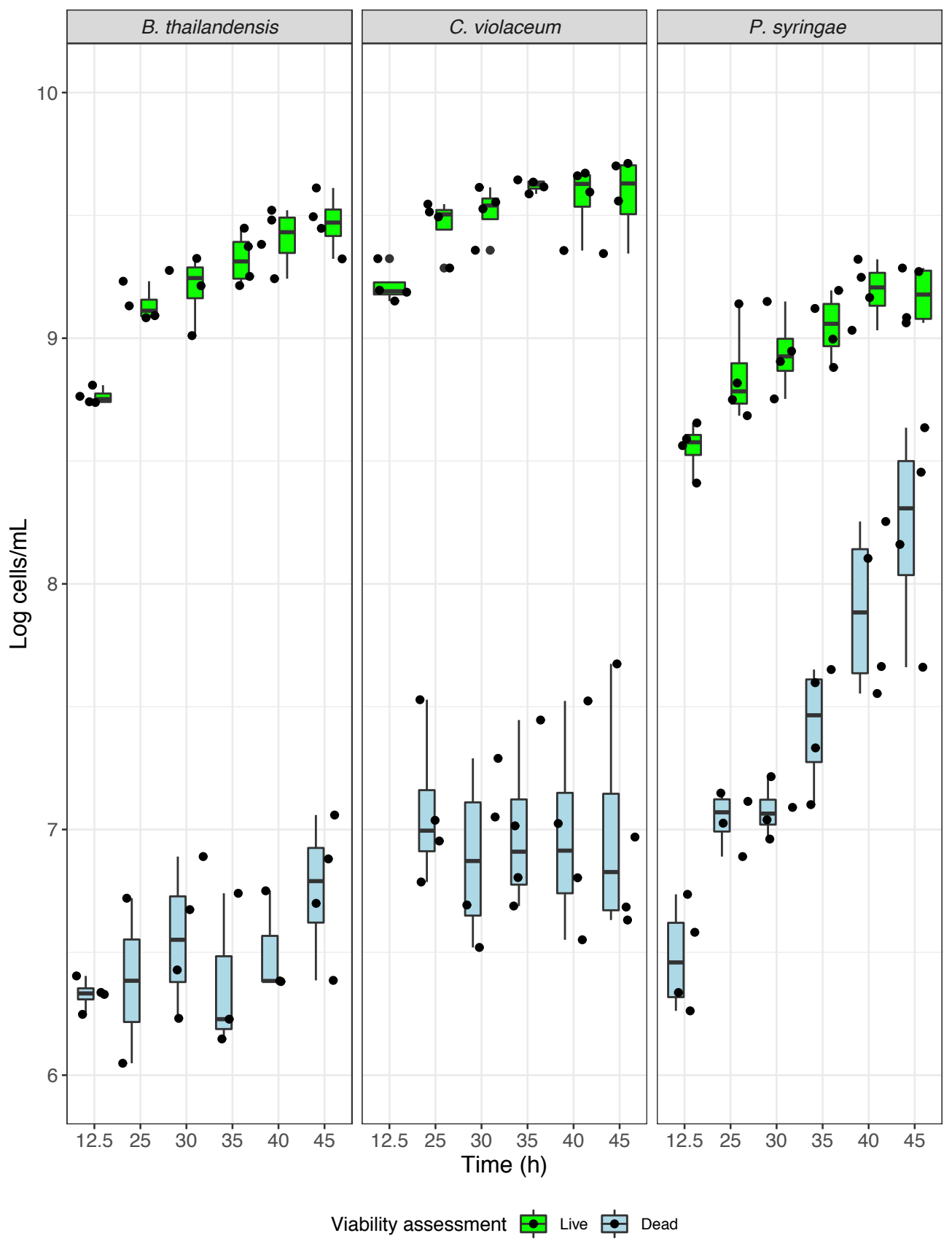
Table 1.

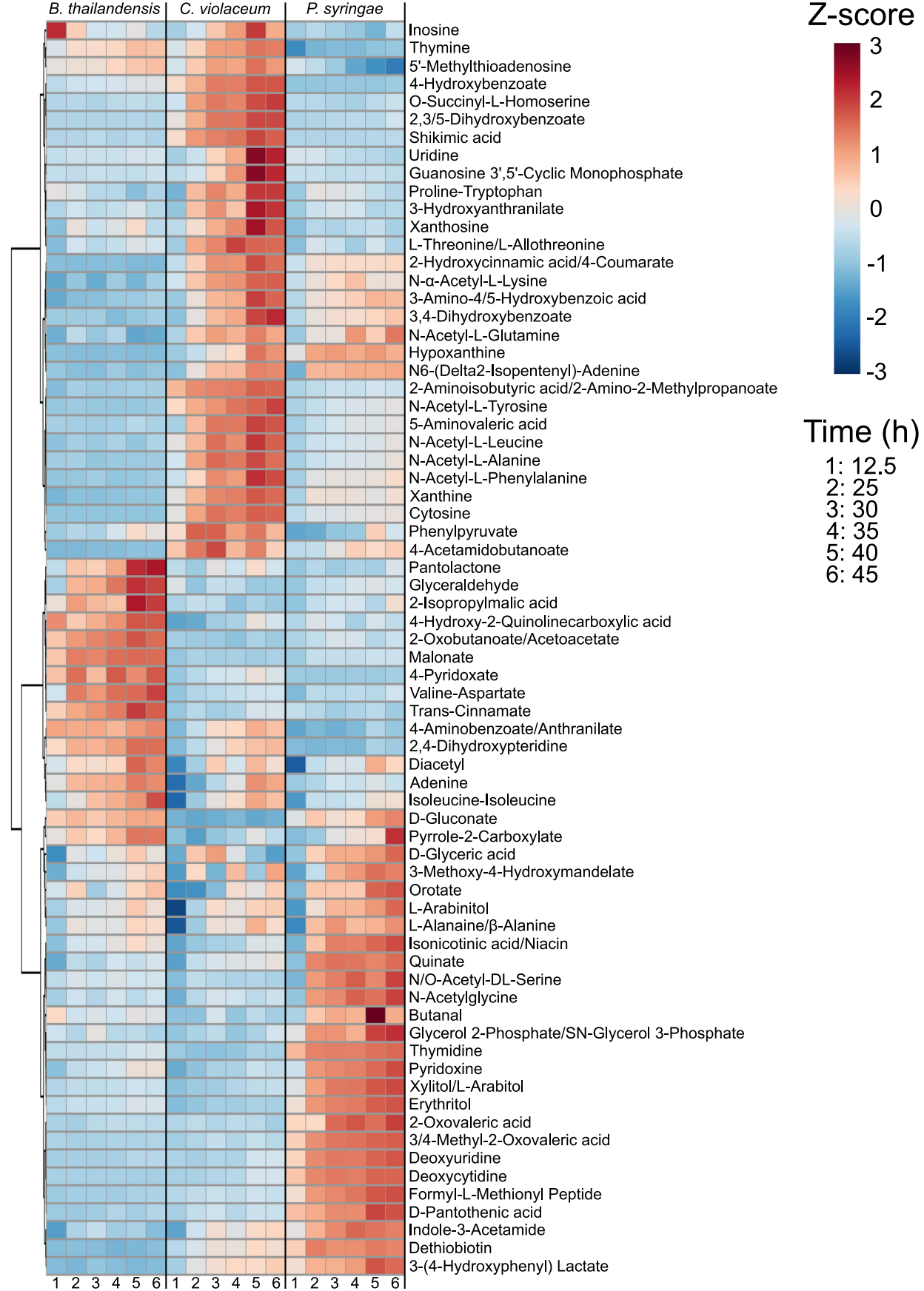
	Family	Genome size (Mb)	ORFs
Burkholderia thailandensis E264 (68)	Burkholderiaceae	6.72	5,641
Chromobacterium violaceum ATCC 31532 (69)	Neisseriaceae	4.75	4,371
Pseudomonas syringae pathovar tomato DC3000 (70)	Pseudomonadaceae	6.53	5,853

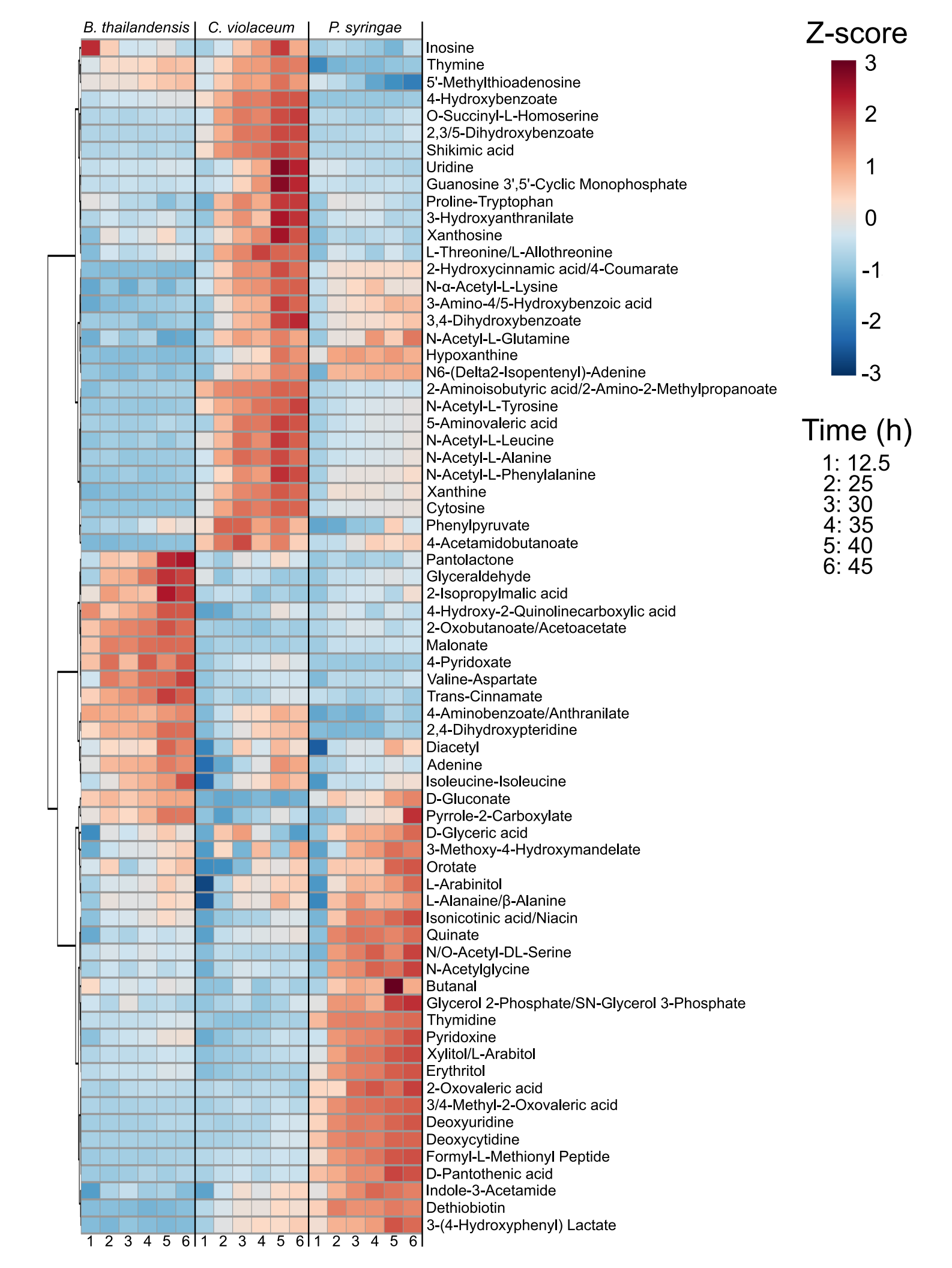
Table 2.

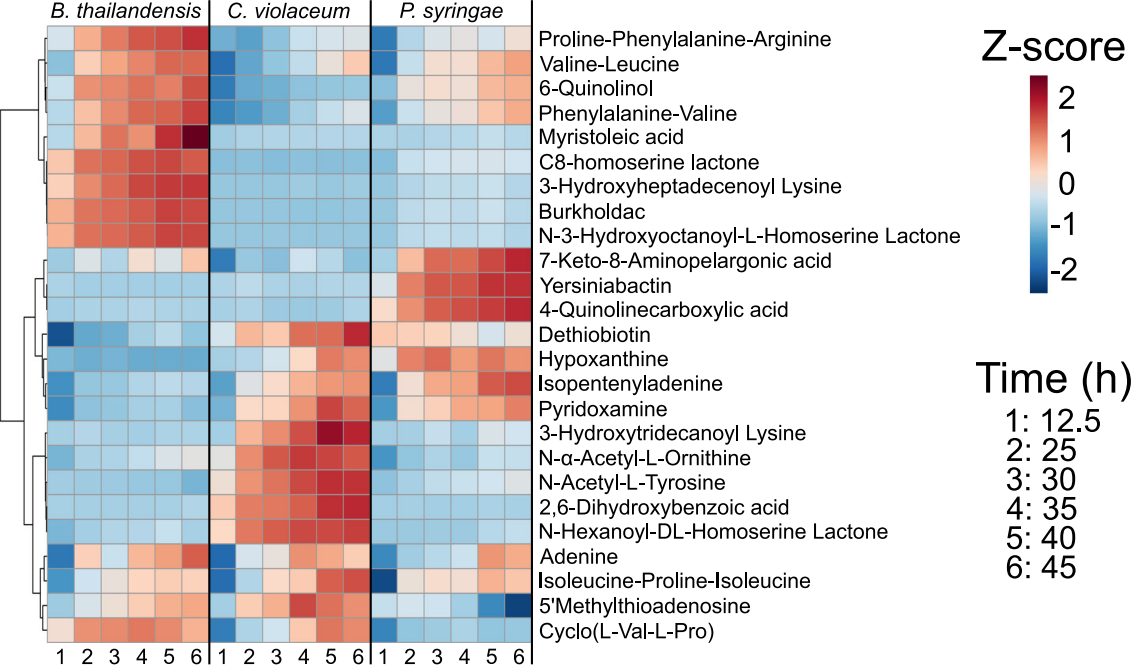
	B. thailandensis	C. violaceum	P. syringae
Total features	5216	3083	3736
Unique features	4327	1922	2609
Features in common with Bt	-	367	333
Features in common with Cv	367	-	605
Features in common with Ps	333	605	-
Features detected in all strains	189	189	189

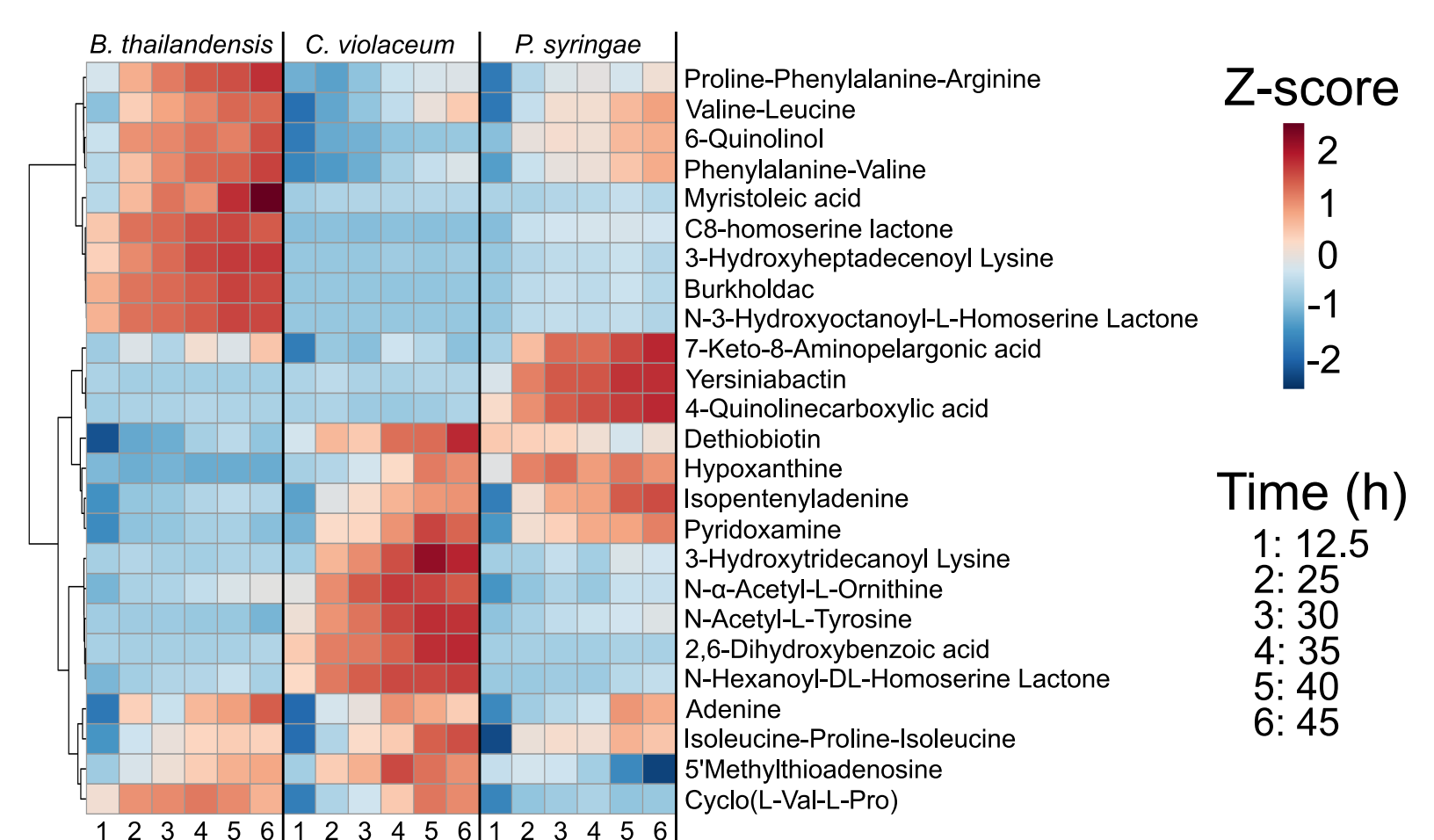


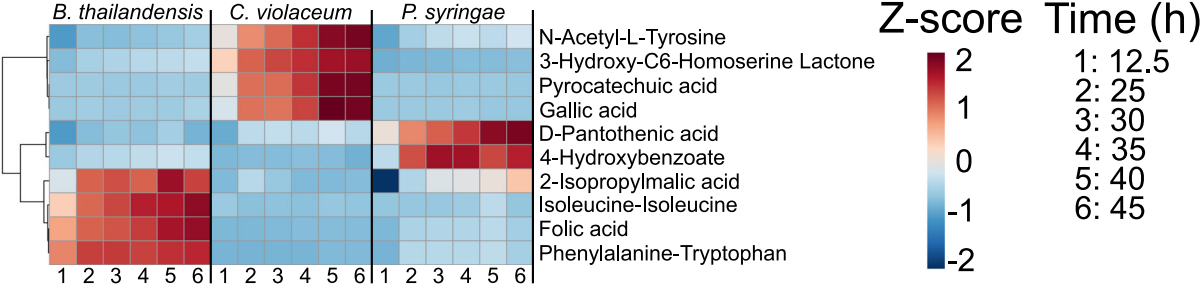


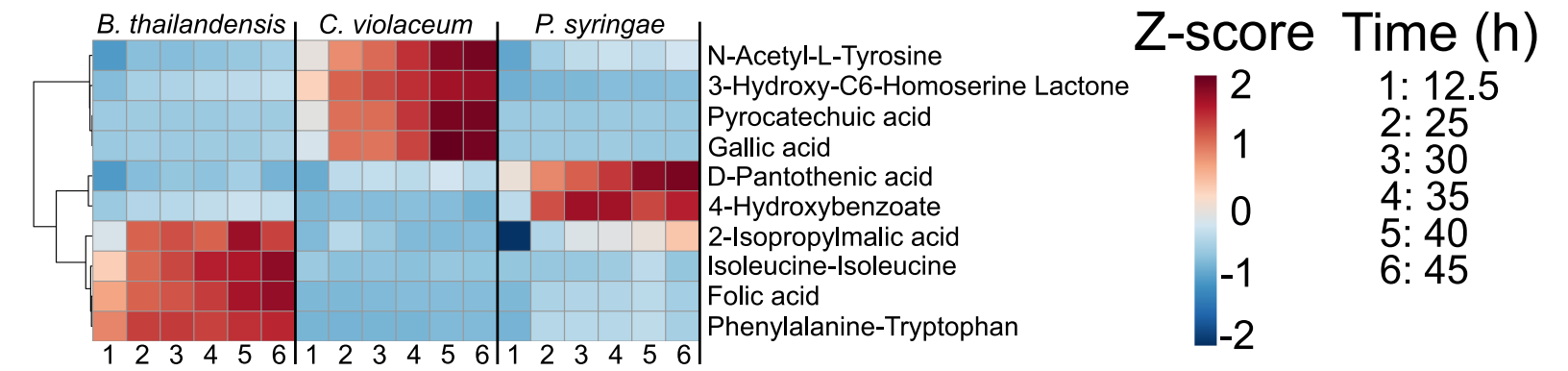












	Strain	Time	Strain x Time
Polar Positive	0.578	0.061	0.685
Polar Negative	0.670	0.026	0.749
Nonpolar Positive	0.762	0.024	0.858
Nonpolar Negative	0.800	0.000	0.865

	m12	R	Р
B. thailandensis	0.019 - 0.389	0.782 - 0.990	0.001 - 0.040
C. violaceum	0.008 - 0.190	0.900 - 0.996	0.001 - 0.035
P. syringae	0.016 - 0.300	0.837 - 0.992	0.001 - 0.075

Time (h)	B. thailandensis	C. violaceum	P. syringae
25	0.132 - 0.181	0.232 - 0.378	0.233 - 0.374
30	0.148 - 0.215	0.298 - 0.382	0.303 - 0.436
35	0.179 - 0.265	0.326 - 0.442	0.339 - 0.458
40	0.218 - 0.323	0.381 - 0.521	0.370 - 0.506
45	0.242 - 0.333	0.361 - 0.526	0.391 - 0.519

Time comparisons (h)	B. thailandensis	C. violaceum	P. syringae
25 to 12.5	0.132 - 0.181	0.232 - 0.378	0.233 - 0.374
30 to 25	0.036 - 0.056	0.035 - 0.112	0.070 - 0.096
35 to 30	0.041 - 0.064	0.042 - 0.078	0.032 - 0.058
40 to 35	0.029- 0.083	0.066 - 0.097	0.049 - 0.075
45 to 40	0.023 - 0.052	0.023 - 0.052	0.036 - 0.057

	B. thailandensis	C. violaceum	P. syringae	
Polar Positive	0.001 (0.553)	0.001 (0.644)	0.001 (0.626)	
Polar Negative	0.068 (0.363)	0.001 (0.650)	0.002 (0.630)	
Nonpolar Positive	0.003 (0.744)	0.002 (0.746)	0.001 (0.892)	
Nonpolar Negative	0.001 (0.849)	0.001 (0.877)	0.001 (0.893)	

Time comparisons (h)	B. thailandensis	C. violaceum	P. syringae
25 to 12.5	0.093 - 0.21	0.088 - 0.15	0.075 – 0.17
30 to 12.5	0.093 - 0.21	0.088 - 0.13	0.075 - 0.17
35 to 12.5	0.093 - 0.21	0.088 - 0.13	0.075 - 0.17
40 to 12.5	0.093 - 0.21	0.088 - 0.15	0.075 - 0.17
45 to 12.5	0.093 - 0.21	0.088 - 0.15	0.075 - 0.17
30 to 25	0.75 - 0.89	0.38 - 1.0	0.15 - 0.79
35 to 25	0.15 - 0.86	0.16 - 0.28	0.15 - 0.72
40 to 25	0.098 - 0.69	0.088 - 0.2	0.075 - 0.59
45 to 25	0.12 - 0.69	0.088 - 0.2	0.086 - 0.40
35 to 30	0.75 - 0.89	0.49 - 0.98	0.64 - 1.0
40 to 30	0.15 - 0.75	0.13 - 0.45	0.15 - 0.79
45 to 30	0.15 - 0.75	0.11 - 0.59	0.15 - 0.60
40 to 35	0.38 - 0.96	0.16 - 0.56	0.46 - 0.97
45 to 35	0.27 - 0.96	0.15 - 0.88	0.38 - 0.83
45 to 40	0.90 - 0.96	0.87 – 1.0	0.94 – 1.0

	Strain	Time	Strain x Time
Polar Positive	0.578	0.061	0.685
Polar Negative	0.670	0.026	0.749
Nonpolar Positive	0.762	0.024	0.858
Nonpolar Negative	0.800	0.000	0.865

	m10	D	
D (1 - 1 - 1 1 1 1 1 1 1 1 1 1 1 - 1 1 1 1 1 1 1 1 1 1 1 - 1 1 1 1 1 1 1 1 1 1 1 - 1 1 1 1 1 1 1 1 1 1 1 - 1 1 1 - 1 1 - 1 1 - 1	m12	R	P 0.004 0.040
B. thailandensis	0.019 - 0.389	0.782 - 0.990	0.001 - 0.040
C. violaceum	0.008 - 0.190	0.900 - 0.996	0.001 - 0.035
P. syringae	0.016 - 0.300	0.837 - 0.992	0.001 - 0.075

Time (h)	B. thailandensis	C. violaceum	P. syringae
25	0.132 - 0.181	0.232 - 0.378	0.233 - 0.374
30	0.148 - 0.215	0.298 - 0.382	0.303 - 0.436
35	0.179 - 0.265	0.326 - 0.442	0.339 - 0.458
40	0.218 - 0.323	0.381 - 0.521	0.370 - 0.506
45	0.242 - 0.333	0.361 - 0.526	0.391 - 0.519

Time comparisons	B. thailandensis	C. violaceum	P. syringae
(h)	0.400 0.404	0.000 0.070	0.000 0.074
25 to 12.5	0.132 - 0.181	0.232 – 0.378	0.233 – 0.374
30 to 25	0.036 - 0.056	0.035 - 0.112	0.070 - 0.096
35 to 30	0.041 – 0.064	0.042 - 0.078	0.032 - 0.058
40 to 35	0.029- 0.083	0.066 - 0.097	0.049 - 0.075
45 to 40	0.023 - 0.052	0.023 - 0.052	0.036 – 0.057

	B. thailandensis	C. violaceum	P. syringae
Polar Positive	0.001 (0.553)	0.001 (0.644)	0.001 (0.626)
Polar Negative	0.068 (0.363)	0.001 (0.650)	0.002 (0.630)
Nonpolar Positive	0.003 (0.744)	0.002 (0.746)	0.001 (0.892)
Nonpolar Negative	0.001 (0.849)	0.001 (0.877)	0.001 (0.893)

Time comparisons	B. thailandensis	C. violaceum	P. syringae
(h)			
25 to 12.5	0.093 - 0.21	0.088 - 0.15	0.075 – 0.17
30 to 12.5	0.093 - 0.21	0.088 - 0.13	0.075 – 0.17
35 to 12.5	0.093 - 0.21	0.088 - 0.13	0.075 – 0.17
40 to 12.5	0.093 - 0.21	0.088 - 0.15	0.075 – 0.17
45 to 12.5	0.093 - 0.21	0.088 - 0.15	0.075 - 0.17
30 to 25	0.75 - 0.89	0.38 - 1.0	0.15 - 0.79
35 to 25	0.15 - 0.86	0.16 - 0.28	0.15 - 0.72
40 to 25	0.098 - 0.69	0.088 - 0.2	0.075 - 0.59
45 to 25	0.12 - 0.69	0.088 - 0.2	0.086 - 0.40
35 to 30	0.75 - 0.89	0.49 - 0.98	0.64 - 1.0
40 to 30	0.15 - 0.75	0.13 - 0.45	0.15 - 0.79
45 to 30	0.15 - 0.75	0.11 - 0.59	0.15 - 0.60
40 to 35	0.38 - 0.96	0.16 - 0.56	0.46 - 0.97
45 to 35	0.27 - 0.96	0.15 - 0.88	0.38 - 0.83
45 to 40	0.90 - 0.96	0.87 - 1.0	0.94 – 1.0

Table 3.

	B. thailandensis			C. violaceum		P. syringae			
Genes involved in transport	669			465		689			
	447ª	103 ^{a,b}	20 ^{a,b,c}	354ª	169 ^{a,b}	53 ^{a,b,c}	461ª	136 ^{a,b}	12 ^{a,b,c}
Genes annotated as transporters related to dipeptide/C4- dicarboxylate transport	26			22		43			
	17ª	4 ^{a,b}	0 ^{a,b,c}	22ª	7 ^{a,b}	1 ^{a,b,c}	20ª	10 ^{a,b}	O ^{a,b,c}
Genes annotated as transporters related to dipeptide/C4- dicarboxylate transport (transcripts below LEM)	9			0		23			

^aAbove LEM

^bDifferentially expressed (Q-value < 0.01)

^cLFC > 1